RADIATION-INDUCED OSTEOPOROSIS: A LOOK INTO THE CHANGES IN
TRABECULAR BONE AFTER EXPOSURE TO ACUTE AND FRACTIONATED
IONIZING RADIATION USING MICE MODEL

Eric W. Lai

A thesis submitted to the faculty at the University of North Carolina at Chapel Hill in partial
fulfillment of the requirements for the degree of Master of Science in the Joint Department of
Biomedical Engineering in the School of Medicine.

Chapel Hill
2018

Approved by:

Caterina Gallippi

Shawn Gomez

Anthony Lau

ABSTRACT

Eric W. Lai: Radiation-Induced Osteoporosis: A Look Into the Changes in Trabecular Bone
After Exposure to Acute and Fractionated Ionizing Radiation Using Mice Model
(Under the direction of Caterina Gallippi)

Radiation therapy is an important tool in the treatment of women with gynecologic cancers. An increased incidence of spontaneous hip fractures is observed in women after receiving therapeutic irradiation.

In this study, we explored the relationship between dosage and bone health by exposing sixteen-week-old C57BL6/J mice to both acute and fractionated dosages of ionizing radiation. The mice were divided into three groups – 18 Gy single acute dose, 3 x 6 Gy fractionated dose and non-irradiated controls. Bones were collected 14 days after irradiation. MicroCT and finite element analyses were used to characterize microarchitectural and structural changes in the proximal metaphysis of the tibia.

Trabecular volume, connectivity density and bone mineral density all declined in the irradiated groups. The fractionated dose group did not demonstrate different bone loss than the single acute dose group in a statistically significant way. Further work is required to elucidate the complex relationship between single acute dose and its fractionated counterpart.

To my parents, grandma and my favorite and only sister, this would not have been possible without you. Thank you for all your love and support.

ACKNOWLEDGEMENTS

TABLE OF CONTENTS

LIST OF TABLES

LIST OF FIGURES

LIST OF ABBREVIATIONS

BMD   bone mineral density

BMP   bone morphogenetic protein

BV/TV   trabecular bone volume fraction

ConnD   connectivity density

DNA   deoxyribonucleic acid

DXA   dual-energy X-ray absorptiometry

EBRT   external beam radiation therapy

FEA   finite element analysis

FRAX   The WHO Fracture Risk Assessment Tool

Gy   Gray (1 Gy = 1 J/Kg)

HRCT   high resolution computed tomography

IRR   irradiated

Micro-CT, μCT   micro computed tomography

MRI   magnetic resonance imaging

NR   non-irradiated

QCT   quantitative computed tomography

REM   roentgen equivalent man (1 rem = 0.01 Sv)

ROI	region of interest
Sv	Sieverts
TBI	total body irradiation
TbN	trabecular number
TbSp	trabecular spacing or separation
TbTh	trabecular thickness
vBMD	volumetric bone mineral density

CHAPTER 1: INTRODUCTION AND MOTIVATION

Radiation therapy or radiotherapy is an established cancer treatment modality and is estimated to be used in 50%-60% of all cancer cases (Beyzadeoglu, 2010). There are two major methods of delivering radiation therapy. The first method, external-beam radiation therapy (EBRT), uses an irradiator machine that is located outside the patient's body. The second method, brachytherapy, places radioactive material inside the body near the cancer cells (Halperin et al., 2013). In both cases, collateral damage in healthy, noncancerous tissues following therapeutic irradiation is an unfortunate side-effect that immensely impacts the quality of life and long-term survival of cancer patients. In particular, irradiation of healthy bone tissues during cancer therapy can result in atrophy and increased risk of fracture at several skeletal sites, particularly the hip (Willey et al., 2010). In the U.S., over 300,000 hospitalizations per year are directly caused by hip fractures. For senior citizens, hip fractures have a 24% mortality rate within the first year. In addition, there is a 250% increased risk of fracture at another site in patients suffering from hip fractures (Shuler et al., 2012).

As more cancer patients undergo radiation therapy with increasing success in initial survival, it has become increasingly important to prevent and minimize long-term risk of bone fractures from the very treatments that are keeping the patients alive (Green and Rubin, 2014; Hu et al., 2007). In 2017, the American Cancer Society estimated approximately 1.7 million new cancer diagnoses in the U.S. alone, with roughly 850,000 new cases for each gender. Of these, cancers in the pelvic region (urinary, genital, colorectal and anal) accounted

for approximately 42% in men and 26% in women. Half of the new diagnoses in women, accounting for over 100,000 new annual cases, could be attributed to gynecological cancers (ACS, 2017; Siegel et al., 2017). Gynecological cancers encompass five main types of cancer that affect a woman's reproductive organs: cervical, ovarian, uterine, vaginal and vulvar. The typical treatment plans for all five types of gynecological cancers use a combination of surgery, radiation and chemotherapy, with staging and tumor size as the determining factors (Beyzadeoglu, 2010; Halperin et al., 2013; Usmani et al., 2005). In early stages where the cancerous cells are localized with limited tumor sizes, invasive surgical removal is the primary treatment modality and is typically followed by radiation therapy to kill any remaining cancer cells (Morris et al., 1999). In later stages that involve significantly larger tumor sizes and/or metastasis of the disease, radiation combined with chemotherapy is used both before surgery to shrink the tumors for more effective removal, and after surgery to treat the remaining affected regions (Rotman et al., 2006). Risk factors for gynecological cancers increase with age (Halperin et al., 2013). When combined with the age-related bone loss or osteoporosis, radiation therapy associated with gynecological cancers puts older women who are pre- or post-menopausal at a particularly high risk for dangerous hip fractures (Oh et al., 2015). For example, women treated for early stage pelvic tumors from gynecological cancers have exhibited a greater than 65% increased incidence of hip fracture five years after completing radiation therapy, causing a substantial increase in morbidity and mortality (Baxter et al., 2005; Willey et al., 2011).

One way to minimize radiotherapy's collateral damage to healthy cells is to break up the total radiation dose and administer it to the patient in smaller doses spread out over time. This process is called fractionation. This allows time for the healthy cells to repair damages,

as cancerous cells have poorer rate of recovery. In addition, certain stages of the cell cycle may provide some radiation resistance qualities (Hall and Giaccia, 2012). Fractionation allows the cancerous cells that survived the initial dose from being in the less radiosensitive stages to progress to a different stage of the cell cycle that is more vulnerable to radiation. The typical radiation therapy dosage for cervical cancer ranges from 40 Gy to 70 Gy, with a median treatment dosage of 45 Gy (Matsuura et al., 2007; Morris et al., 1999). For adults, the overall dosage is usually administered in daily fractions of 1.8 Gy – 2.0 Gy. For children, the daily fractions are typically slightly lower at 1.5 Gy – 1.8 Gy. In the United States, a general rule of thumb for fractionated irradiation is dividing the total desired dosage into 30 equal fractions, administered five consecutive days per week over six weeks (Pollack and Ahmed, 2011). However, there really is not one typical fractionation schedule. Treatment regimens can differ from one disease to another, one oncologist to another, and even one patient to another (Cho et al., 2005; Khalil et al., 2003).

Overall Goal and Hypothesis

The work presented in this manuscript is motivated by two main reasons: the prevalence and importance of radiation therapy in modern cancer treatment regimen, and the significant increase in morbidity and mortality in cancer patients from increased fracture risk. The goal of this study is to develop an animal model to explore and characterize the differences in the effects between single acute dose versus fractionated dosage on healthy bone tissues. The active growth region of the tibia will be the focus, and any potential bone loss will be characterized and quantified in terms of structural changes, bone mineral density and various trabecular bone parameters obtained through micro-computed tomography or micro-CT. In addition, finite element analysis will be used toobtain insights into the effects

of microstructural changes have on overall bone strength. Our hypothesis is that ionizing radiation administered in fractionated dosages will have a less deleterious effect on healthy bone tissues compared to the equivalent dosage given in one single acute dose.

We hope the insights obtained from this work will shed additional light on the intricate relationship between ionizing radiation and bone loss, ultimately leading to improvements in both the efficacy of gynecological cancer radiation therapy and quality of life for the cancer patients.

CHAPTER 2: BACKGROUND

General Bone Physiology

In the human body, bones serve five major functions: protection of vital organs, structural support for the entire body, blood production in the bone marrow, vital mineral storage, and framework to enable movement by working with skeletal muscles, tendons and ligaments to allow for transfer of force. Typically, bones are classified by their shapes. This results in five major types of bones: long, short, flat, irregular and sesamoid (Allen and Burr, 2014; Moore and Dalley, 2006). Long bones are subjected to the majority of the load during normal daily activities and therefore essential to basic skeletal mobility. For this manuscript, we will focus on long bones, since their load-bearing status leads to a higher risk of fracture. We will discuss basic bone anatomy, three types of bone cells and the bone remodeling cycle.

Basic Bone Anatomy

The two basic bone structures are cortical and trabecular bone. Cortical bone, also known as compact bone, is the dense hard outer shell that make up about 80% of the adult skeleton's total bone mass with a porosity of 5%-10%. It provides excellent compressive strength and resistant to bending and torsion (Allen and Burr, 2014). The overall remodeling rate is about 2% - 5% per year in healthy adults. As a result, cortical bone is found in areas that are load-bearing or need protection, such as the vertebrae, shaft of long bones and the skull.

Trabecular bone, also known as cancellous or spongy bone, is composed of thin interconnected struts that make up the porous structure inside the cortical shell. These struts or trabeculae account for the remaining 20% of the adult total bone mass with a 50% - 90% porosity (Burr and Akkus, 2014; Moore and Dalley, 2006). Trabecular bone adds mechanical support by directing the load forces to the stronger outer cortical bone. This allows for deformation and helps the bone as a whole to absorb load forces more efficiently with minimal increase in overall bone weight (Moore and Dalley, 2006). With its larger surface area compared to cortical bone, trabecular bone has a higher rate of bone turnover that allows for structural remodeling. In response to the location and direction of loading, trabecular bone will optimize its number and thickness to maximize bone strength. Reduction in connectivity or trabecular number reduces bone stiffness by up to 300% more than reduction in trabecular thickness alone (Burr and Akkus, 2014).
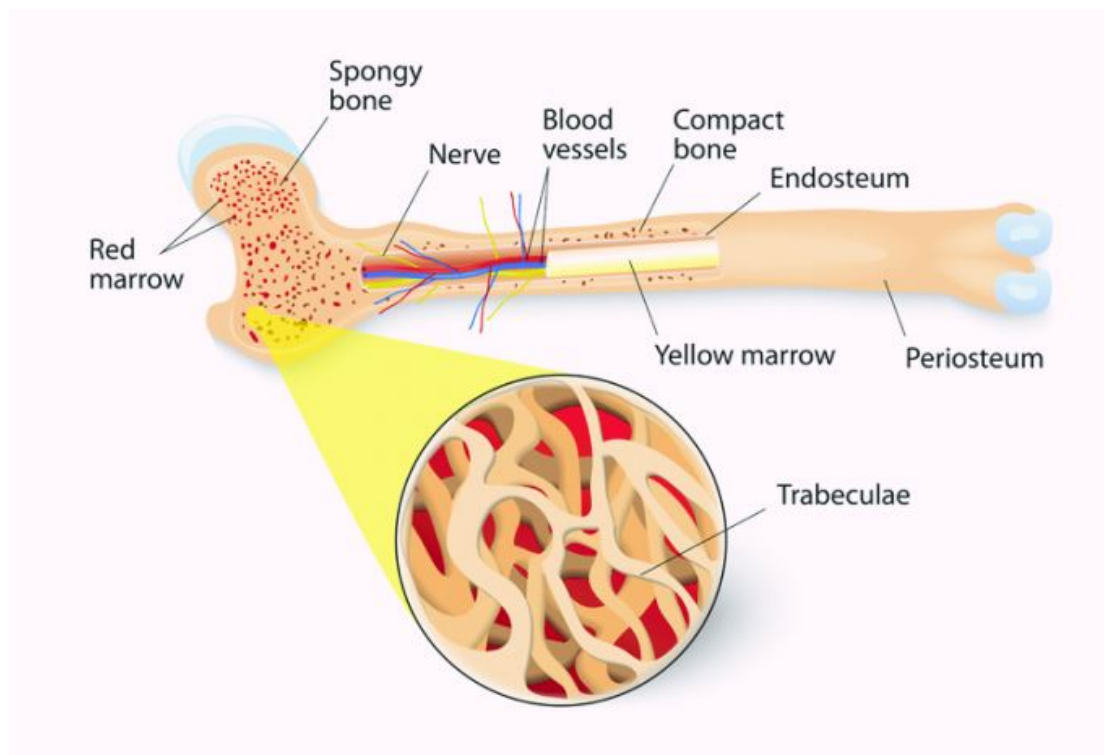

Figure 1: Basic bone anatomy

Bone marrow is the soft, gelatinous tissue found in the medullary cavities inside the cortical shell. There are two types: red and yellow. Red bone marrow contains hematopoietic stem cells or blood-forming stem cells. They give rise to red blood cells (erythrocytes), white blood cells (leukocytes) and platelets (thrombocytes). In long bones, red marrow is found among the trabecular bone. Yellow bone marrow contains mesenchymal stem cells, which give rise to fat, cartilage and bone cells. In humans, bone marrow remains red until around the age of 7, due to the high need of blood formation during early development. Yellow bone marrow gradually replaces the red marrow as the body ages beyond age 7. There is on average approximately 2.6 kg of bone marrow in an adult human, with a 50/50 ratio of red and yellow marrow (Moore and Dalley, 2006; Nichols, 2017).

The outside and inside of the bone are covered with fibrous membranes called the periosteum and endosteum, respectively. These membranes, rich with capillaries, are responsible for nourishing the external and internal aspects of the bone (Netter, 1987).
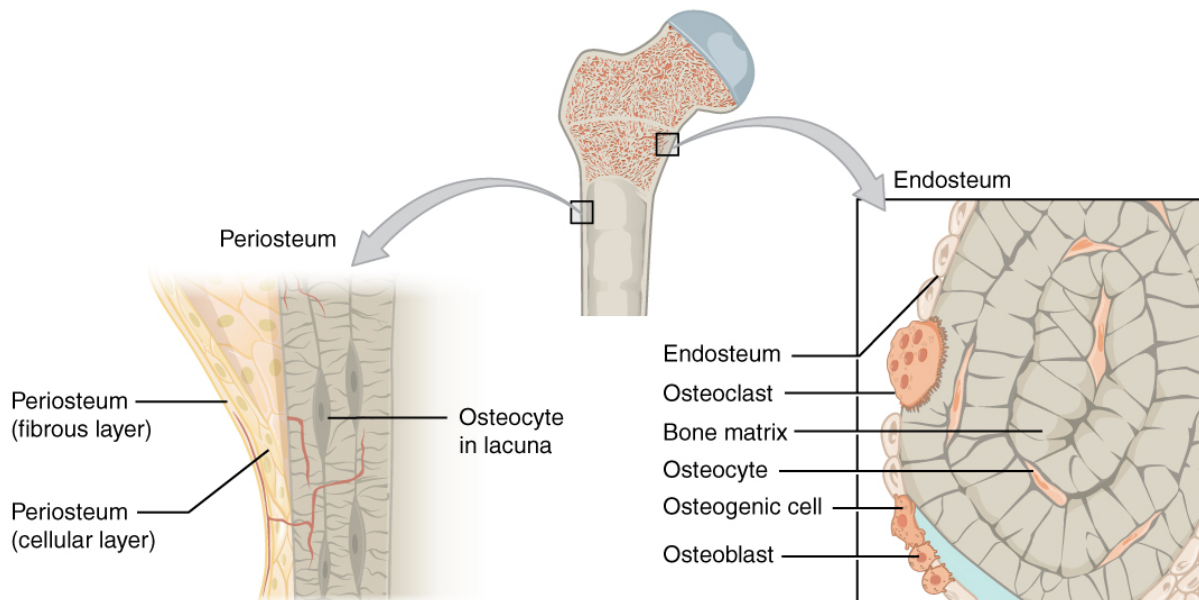
Figure 2: Periosteum and endosteum

Long bones, such as the femur and tibia, contain a hard outer cortical shell, a cancellous trabecular inner structure and a bone marrow cavity. The long shaft is called the diaphysis. It is composed of primarily thick cortical bone and contains the cavity for yellow bone marrow in human adults. The metaphysis is found at the end of the diaphysis. It contains red bone marrow and trabecular bone enclosed by a thin cortical shell. The epiphysis is the rounded head at each end of the bone. It contains trabecular bone enclosed by a relatively thin cortical shell. The growth plate, also known as the epiphyseal plate, is found between the epiphysis and metaphysis. During periods of growth, long bones grow outward from the growth plates. Once growth is complete, the plate closes and is replaced by solid bone.

Figure 3: The anatomy of the osteon

The microscopic unit that makes up the bulk of cortical bones is called the osteon, which consists of concentric lamellae organized around Haversian canals. These canals

8

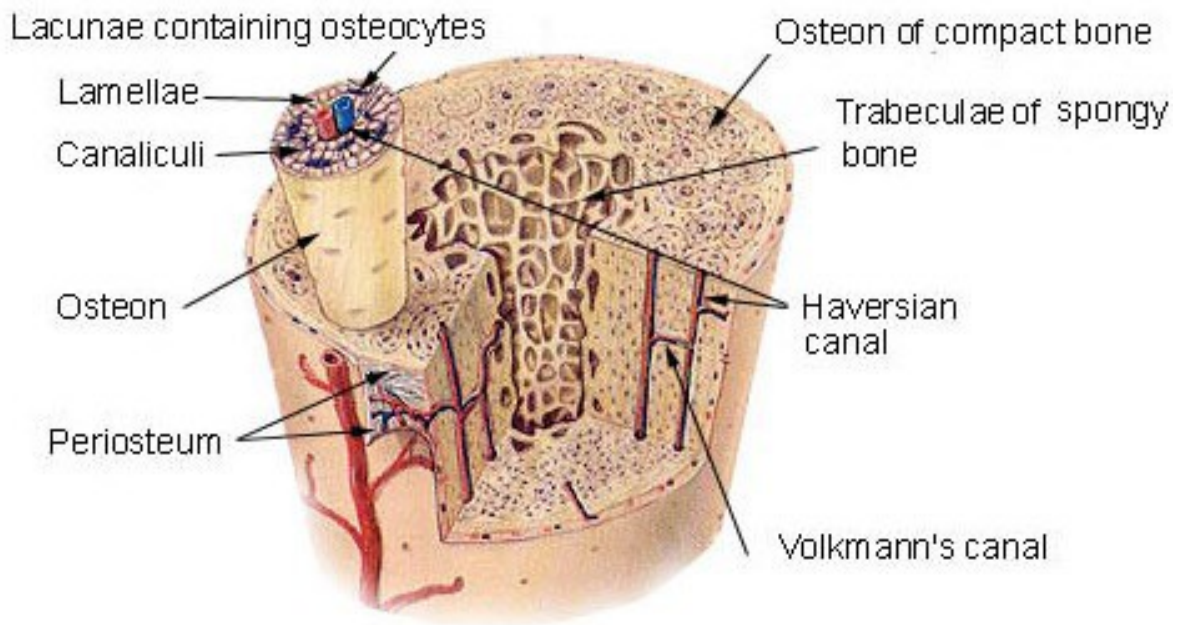provide the necessary channel for nerves and blood vessels, and appear as dark circular holes in bone cross sections. Canaliculi, small dots that contain osteocytes and surround the Haversian canal, are visible cues for lamellar boundaries. The outermost boundary of a lamella is the cement line, and it indicates where bone resorption has stopped. Cement lines function as barriers to microcrack propagation and help to maintain the osteon's structural integrity on a microscale (Burr and Akkus, 2014).

Bone Cells

There are three main types of bone cells: osteoblasts, osteocytes and osteoclasts. Each serves a distinct function and interacts with each other via various signal pathways to form the basis for the bone remodeling process.

Osteoblasts

Osteoblasts are responsible for bone formation. They achieve this through secretion of bone matrix protein osteocalcin and rapid production of type I collagen to form osteoid, which is the unmineralized precursor to the mature and fully mineralized bone tissue (Bellido, 2014). The osteoblast lifecycle starts with mesenchymal stem cells that develop into osteoprogenitor or preosteoblastic cells. Once they adhere to the bone matrix, alkaline phosphatase is secreted. This is followed by the expression of type I collagen and the secretion of the extracellular matrix. At the onset of calcification, the osteoblast cells secret osteocalcin, osteonectin, osteopontin, bone sialoprotein and other products (Marie, 1998). Once the bone matrix synthesis is complete, osteoblast cells will either undergo apoptosis or flatten and cover the bone surface, eventually becoming embedded in the newly formed bone matrix. At this point, the embedded osteoblasts become osteocytes (Bellido, 2014).
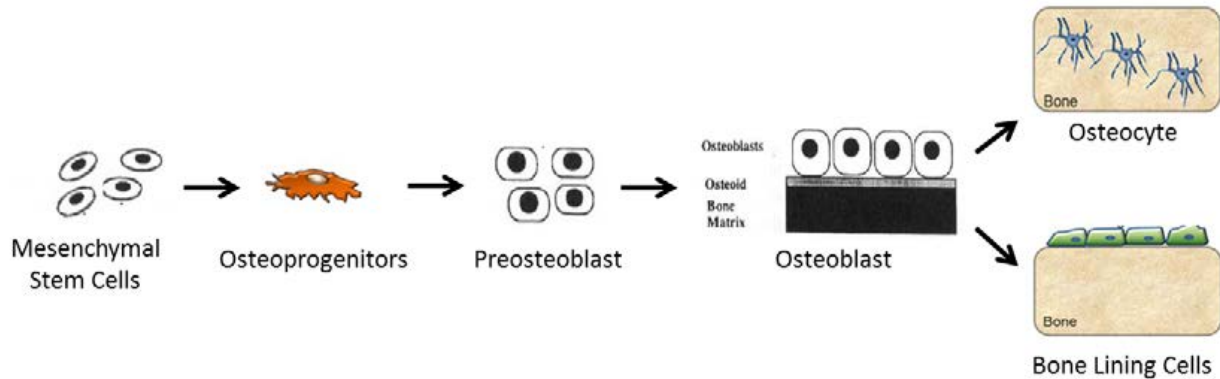
Figure 4: The osteoblast lifecycle

Various signaling pathways and proteins regulate the osteoblast's proliferation and differentiation. Wnt pathways are instrumental in signaling mesenchymal stem cells to start down the osteoblastic pathway. They also play a role in stimulating the differentiation of preosteoblasts and the inhibition of osteoblastic apoptosis. Another signaling pathway is the bone morphogenetic protein (BMP), which controls osteoblast differentiation, promotes bone matrix protein synthesis and induces cell apoptosis at the end of the cycle (Bellido, 2014; Marie, 1998). Mature osteoblasts produce insulin-like growth factor (IGF), fibroblast growth factor (FGF) and transforming growth factor beta (TGF-β) to expedite osteoblastic precursor cells. Prostaglandins and IGF stimulate the proliferation of osteoblasts and encourage bone collagen synthesis (Marie, 1998).

Osteocytes

Osteocytes are mature osteoblasts that have become flattened and embedded in the newly formed bone matrix. They develop long dendrites that extend into the bone matrix and are responsible for starting the bone remodeling process in response to mechanical loading or microcracks. Osteocytes use their long dendrites to monitor the health of the bone matrix and to form a network with other osteocytes, enabling an extensive signaling and protein

exchange pathway. Like osteoblasts, osteocytes also secrete proteins that stimulate mineralization, including osteocalcin and alkaline phosphatase (Bellido, 2014).

The lifecycle of osteocytes consists of four stages: formative, steady-state, resorptive and degenerative. In the formative stage, flattened osteoblasts embed themselves into the newly formed bone matrix. In steady-state, the osteocyte lies dormant with very little metabolic activity. This is followed by the resorptive stage where the osteocyte remodels surrounding matrix. Finally, the osteocyte dies in the degenerative stage (Aarden et al., 1994).

Osteoclasts

The main responsibility of osteoclasts is bone resorption, or the breaking down of bones. They are multinucleated and use an unique bone-cell interface consisting of filamentous actin structures called podosomes to attach to bones (Bellido, 2014). Bone resorption is conducted through a H+ adenosine triphosphate mediator in an exocytosis-like process (Teitelbaum, 2000). Hydrolytic enzymes are secreted to acidify and break down the bone matrix. The degraded bone fragments are processed and discharged by the osteoclast. The final result of the bone resorption process is a pit called Howship's lacunae (Bellido, 2014).

Bone Remodeling Cycle

The bone remodeling process is the sum of the activities by the osteoblast, osteocyte and osteoclast. It forms the foundation for the life cycle of bone tissues. There are five stages: activation, resorption, reversal, formation and quiescence (Allen and Burr, 2014).

Bone Remodeling Cycle
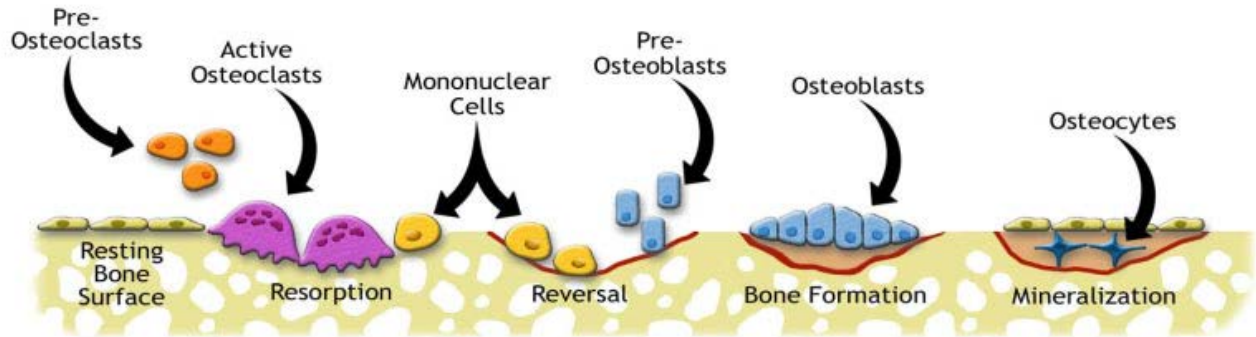
Figure 5: The bone remodeling cycle

In the activation stage, one or more dying or damaged osteocyte releases RANKL and various other factors to prompt osteoclast activity. Preosteoclasts follow the signal and start to migrate toward the damaged location in the bone. Healthy osteoctyes nearby release antiapoptotic signals to protect healthy bone tissues and limit resorption to only the damaged region (Allen and Burr, 2014).

Resorption starts when the preosteoclasts become mature osteoclast cells. They signal the bone lining cells to allow for attachment to the damaged region. Once attached, osteoclasts secrete hydrolytic enzymes to break down the bone matrix and digest the degraded tissues. The result is a Howship's lacuna (Bellido, 2014).

In the reversal stage, macrophages signals preosteoblasts and prepare the Howship's lacuna for new bone formation. When this stage is finished, mature osteoblasts begin the bone formation process by secreting type 1 collagen and other bone matrix proteins. Mineralization follows when solid calcium phosphate crystals are formed from the soluble

calcium and phosphate in the newly formed bone matrix. At this point, osteoblasts either undergo apoptosis or become flattened and embedded, eventually maturing into osteocytes (Allen and Burr, 2014). Finally, the bone enters the quiescence stage.

The biomarkers associated with the bone remodeling cycle are summarized in table 1.

Molecule	Abbreviation	Matrix	Source
Formation			
Osteocalcin*	OC	Serum	Allen 2014, Christenson, 1997
Bone-specific alkaline phosphatase	BSAP, BALP	Serum	Allen 2014, Christenson 1997
Procollagen type I N propeptide	PINP	Serum	Allen 2014, Christenson 1997
Procollagen type I C propeptide	PICP	Serum	Christenson 1997
Resorption			
Tartrate-resistant acid phosphatase	TRAP	Serum	Allen 2014, Christenson 1997
Pyrindoline	PYD	Urine	Allen 2014
Deoxypyrindoline	DPD	Urine and serum	Allen 2014, Christenson 1997
Osteoprotegerin	OPG		Plotkin 2014
N-terminal cross-linking telopeptide of type I collagen	NTX-I	Urine and serum	Allen 2014, Christenson 1997
C-terminal cross-linking telopeptide of type I collagen	CTX-I	Urine and serum	Allen 2014, Christenson 1997
Urinary calcium		Urine	Christenson 1997

Table 1: Common biomarkers associated with bone formation and resorption (Allen and Burr, 2014)

Osteoporosis

Osteoporosis is a disease of the bones that stems from an imbalance between the activities of the osteoblasts and osteoclasts, cells that are responsible for bone formation and resorption, respectively. In a patient with osteoporosis, the overall bone turnover rate is skewed toward net resorption, resulting in the loss of bone mineral density and alterations in the bone microstructure. These changes ultimately decrease overall bone strength and increase the risk for formation of fractures that otherwise would not form. Over 70 million people worldwide are at risk of developing osteoporotic fractures. Depending on the location, fractures from osteoporosis can lead to reduced mobility, disability or even early mortality

(Damilakis et al., 2010; NIH Consensus Development Panel on Osteoporosis Prevention, 2000; Shuler et al., 2012). Another reason osteoporosis is dangerous is due to the fact that it is often detected only after a spontaneous fracture has taken place (Shuler et al., 2012).

Although commonly associated with older females, osteoporosis occurs in both genders and across all ethnic groups. Conditions that promote the onset of this disease include the lack of estrogen in females and androgen in males, inadequate supply of calcium and/or vitamin D, bone cancer, thyroid diseases, insufficient load-bearing exercises and old age (Green and Rubin, 2014).

The mechanism of osteoporosis involved a net imbalance in the activities of osteoblasts and osteoclasts, where the net resorption rate is higher than that of the formation. Trabecular bones are especially vulnerable to increased bone turnover and resorption (Shuler et al., 2012). As they thin and lose bone mass, trabecular struts eventually lose connection with each other and fail. This results in a decrease in connectivity density (ConnD), and additional loss in bone strength from more than just thinning alone. In addition, once the connection has been broken, it is impossible to reconnect trabecular struts (Allen and Burr, 2014), with the resulting bone becoming weakened and more prone to suffer fractures. This is especially true for regions of the skeletal system with high percentage of trabecular bone, such as the wrist, vertebrae and hip (Allen and Burr, 2014; Damilakis et al., 2010; Shuler et al., 2012). Figure 6 on the following page gives a visual comparison between healthy and osteoporotic trabecular bones.
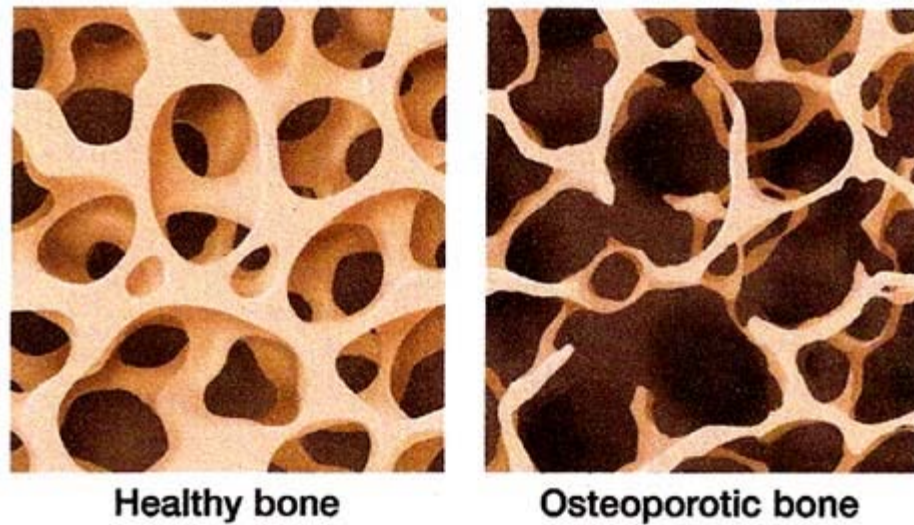
Figure 6: Healthy and osteoporotic trabecular bones

The WHO Fracture Risk Assessment Tool (FRAX) and T-scores are the current standard tools for assessing osteoporosis. With FRAX, potential patients and their associated fracture risks are identified through parameters that include country of origin, age, gender, personal and family history involving fractures, cigarette and alcohol usage, body mass index (BMI), bone mineral density (BMD) and history of rheumatoid arthritis (Shuler et al., 2012). With the T-score, patient's bone mineral density is compared to a young reference population near peak bone mass. Standard deviation values are then used to determine risk level (Damilakis et al., 2010).

Ionizing Radiation

Radiation is defined as energized particle or waves traveling through a medium or space. There are two types of radiation: non-ionizing and ionizing. On one end of the electromagnetic spectrum, the non-ionizing radiation includes examples such as radio waves, heat and visible light. These types of waves are relatively low in energy and do not pose

harm to biological organisms. Ionizing radiation resides on the other end of the electromagnetic spectrum and includes ultraviolet, X-rays and Gamma rays. These types of radiation have much higher energy – enough to successfully knock loose a valence electron from the target material's atomic structure, resulting in the creation of an ion or free radical. Free radicals are very chemically reactive and highly damaging to biological tissues (Hall and Giaccia, 2012).

Radiation is further classified into directly and indirectly ionizing. Direct ionizing radiation has a high enough kinetic energy that it is able to directly disrupt the atomic structure of the absorber it passes through and affects chemical and biological changes. This radiation is less common and includes heavy charged particles. Indirectly ionizing radiation has less kinetic energy and does not produce chemical and biologic damage by itself. Instead, when absorbed by a target, it passes its energy to produce fast-moving charged particles that in turn cause damage (Hall and Giaccia, 2012). Examples of indirectly ionizing radiation include X-rays and Gamma rays.

Biologic effects of radiation primarily result from damage to deoxyribonucleic acid or DNA. There are two mechanisms ionizing radiation can cause harm to DNA. In direct action, the ionizing radiation creates ions that directly impact and damage the DNA structure. These require radiation with high linear energy transfer (LET), such as neutrons and other heavy charge particles. In indirect action, the ionizing radiation creates free radicals that in turn interact with the DNA. One of the most common free radicals is the hydroxyl radical (OH), produced when a water molecule loses one of its oxygen atoms. It is estimated that 2/3 of all damage to mammalian cells are from hydroxyl radicals (Beyzadeoglu, 2010; Hall and Giaccia, 2012).

Ionizing radiation induces multiple forms of damage to the DNA molecule. These include base damage, single and double strand breaks in the DNA helix, and DNA protein crosslinks. Double strand breaks are the most lethal form of ionizing radiation induced damage, and is believed to be the cause of majority of radiation-induced cell death (Beyzadeoglu, 2010; Hall and Giaccia, 2012). The cell has evolved complicated series of sensors and pathways to respond to these radiation-induced damages and attempt to initiate repair. However, cells go through the cell cycle as they propagate and proliferate. The stages of the cell cycle include the mitosis (M) phase, growth phase (G1), DNA synthesis and replication phase (S) and the dormant phase (G2). It is during the time of cell division that the cell is most sensitive to radiation and its induced damage. In terms of the cell cycle, mammalian cells are most radiosensitive in G2 and M phase and most resistant in late S phase (Hall and Giaccia, 2012). The reasons for radiosensitivity changes through the cell cycle are still not fully understood.

The linear-quadratic model is currently the most widely accepted model for describing radiation-induced cell death. Also known as the Fowler equation, it was first introduced in 1972 and still remains as the foundation for relating dose to survival fraction (Douglas and Fowler, 1976; Fowler, 2010):

$$Surviving\ fraction\ (SF) = e^{-\alpha D - \beta D^2}$$

D is the radiation dosage, and α and β are experimental constants. It follows the accepted rationale that double strand DNA breaks are the most lethal, and this could be caused by either a single or double radiation track or encounter. Single track radiation encounter is represented by the first D and double track with D^2. Cell death is thought to follow the Poisson distribution from cell to cell, resulting in the final form of the question.

Mouse Model & Strain

No animal model is perfect, as each carries with it its own advantages and disadvantages. In this study, we chose to use C57BL/6 mice in our animal model for several reasons. Mice have a relatively easily manipulated genome. Their skeletal system is similar to that of the humans. Like humans, mice suffer loss of cancellous or trabecular bone, thinning of the hard outer cortical bone and increased cortical porosity as they age. From histological evidences, both humans and mice have similar pathways for bone loss, mainly through lowered or inadequate osteoblast activities, which results in insufficient refilling of resorption cavities created by the osteoclasts during bone remodeling (Jilka, 2013).

The C57BL/6 strain's age-related bone loss exhibits a remarkably close pattern of response compared to humans. In a longitudinal bone mineral density (BMD) study involving 26 inbred mouse strains, multiple strains showed noticeable variability in age-related bone loss as determined by dual-energy X-ray absorptiometry (DXA) (Ackert-Bicknell C; Maddatu et al., 2012). Between the age of 12 and 20 months, DBA/2 females showed around 4% decrease in BMD. The NZO/HILtJ strain suffered 8% decrease in BMD during the same period. On the other end of the spectrum, RIIIS/J females increased by 10% in BMD during the same period. C57BL/6 mice did not experience a significant change in BMD, by comparison. In addition, there were also differences in bone loss rate between genders in certain strains. But with C57BL/6 mice, the rate of bone loss was similar between 16 and 30 months of age (Almeida et al., 2007). This suggests that insights obtained from this study may be useful in shedding light on radiation-induced osteoporosis and related increase in fracture risk in not only females, but also their male counterparts as well.

CHAPTER 3: METHODS AND RESULTS

Overall Goal and Aims

The overall goal of this study is to gain additional insight into the causal relationship between ionizing radiation and bone loss induced by it in otherwise healthy bone tissues. This will be achieved through the completion of the following aims:

- Develop an animal model to explore and characterize the differences in the effects between single acute dose versus fractionated dosage on healthy bone tissues

- Quantify the amount of bone loss in the spongy trabecular region of the tibia, where the bone growth and remodeling process is the most active

- Examine the role of structural strength in the overall strength of the bone using specimen-specific models in finite element analysis

Methods

This was a 14-day animal study. Thirty-six female, sixteen-week-old C57BL/6 mice were obtained from Charles River Laboratories International, Inc. in Morrisville, NC through National Institute of Aging (NIA). The mice were randomized and divided evenly into three study groups with twelve animals each: NR (non-irradiated control), 18 Gy single acute dose and 3x6 Gy fractionated dose. To monitor general health and well-being, weight for each mouse was measured and monitored at baseline and throughout the duration of the study. Mice exhibiting a 20% or larger decline from their baseline weight within the first three days were deemed under duress and removed from the study as part of the standard animal safety

protocol. The study animals were housed at the animal facility on the campus of the

University of North Carolina at Chapel Hill. Each cage housed 5 animals. Cages were

grouped together based on normalized weights of the mice before being assigned to one of

the three study groups.

The X-Rad 320 Biological Irradiator (Precision X-Ray, North Branford, CT) was

used to deliver the desired radiation dose at 0.5 Gy/minute to the study groups. Pelvic

irradiation started on day 0 for both the 18 Gy single acute dose and 3x6 Gy fractionate dose

groups. The fractionated dose group received the second and third fraction at 72 hour

intervals. During exposure, isoflurane was used to sedate the animals. A custom delivery

piping system was created to ensure a steady and constant delivery of isoflurane into each

mouse inside the X-Rad 320. Once sedated, mice from each cage were placed in the prone

position inside the irradiator. The irradiator's collimator was adjusted to only expose each

animal from the pelvic region downward.

At the end of the study, the study animals were humanely euthanized via cardiac

puncture and exsanguination followed by cervical dislocation. Right tibiae were harvested

from all 36 animals. The bones were cleaned and fixed in formalin for 48 hours before going

into stable storage in 70% ethanol.

Micro-CT analysis (μCT 80; Scanco Medical AG, Bassersdor, Switzerland) of the

tibia was conducted in the 1 mm region of the metaphysis just below the epiphyseal plate.

Images of each sample were obtained with a 10 μm voxel size. Once specimen was scanned,

the cortical and trabecular sections were manually delineated through the creation of contours

or regions of interest. This was followed by segmentation, or the identification of bone

material in the region of interest. A threshold value for mineralized material was used to

accept or reject a voxel as bone material, ideally including all visible bone while excluding all other artifacts. Six trabecular microarchitectural parameters were obtained for analysis: BV/TV (trabecular bone volume fraction), vBMD (volumetric bone mineral density), ConnD (connectivity density), TbTh (trabecular thickness), TbSp (trabecular separation) and TbN (trabecular number).

Finite element analysis was used to analyze the same 1 mm region. Mesh data for both the isolated outer cortical shell and the whole bone including the trabeculae was created from the raw micro-CT images using a voxel-to-element conversion. This data was then exported over to Abaqus (Abaqus/CAE 6.9-EF1, Dassault Systems Simulia Corp, Providence, RI) to create subject specific finite element models. The mesh models were then subjected to a basic compression test with a 0.5% downward displacement (5 µm) to simulate axial compression. Material properties were assumed to be isotropic or homogenous with a Young's modulus of 10 GPa and a Poisson's ratio of 0.3. Of the many variations of axial compression test, we chose to fix the bottom surface and displace the top, as this was sufficient given that the simulated loading was static in nature. To characterize bone strength, we looked at the stiffness, defined as the resultant force divided by the applied displacement. Structural efficiency, defined as stiffness divided by total bone volume, is a way to look at the material strength normalized to unit volume. Stiffness and structural efficiency data were obtained from the 0.5% axial compression tests for analysis.

GraphPad Prism 5.0 (GraphPad Software, San Diego, CA) was used for all statistical analyses. Outliers in the dataset were defined to be any data points that were at least three standard deviations from the mean in either direction. A one-way ANOVA was performed to determine the significance of the dataset, with P-values less than 0.05 considered statistically

significant. Tukey's Honest Significant Difference test was then performed as the multiple comparison test to determine where those significant differences lie.

Results

Body Mass

The weight of each animal was measured and monitored throughout the study. There were no exclusions throughout the study, and the same trend was seen across all three groups. The mean weight for all three groups are shown below.
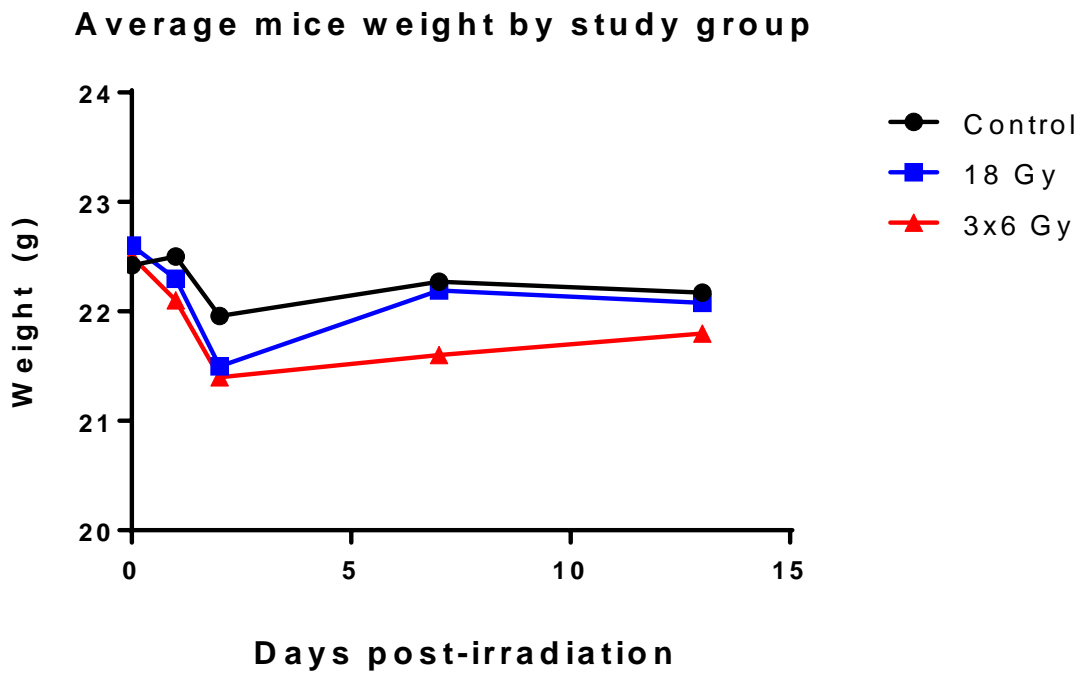

Figure 7: Average mice weight by study group. Note the similar initial drop in weight across all groups, including control.

Trabecular Microarchitectural Parameters

Trabecular Bone Volume Fraction

The trabecular bone volume fraction (BV/TV) is shown below in Figure 8. Results were statistically significant for the 3x6 Gy fractionated group when compared to the control, with a 32.5% decrease in overall trabecular bone volume fraction (p-value = 0.0036). The 18 Gy single acute dose group showed a 17.4% decrease when compared to the control, but it was not deemed statistically significant (p-value = 0.1594). When compared with each other, the two irradiated groups showed some differences, with the 3x6 Gy have on average bigger loss. However, this difference was not deemed statistically significant.
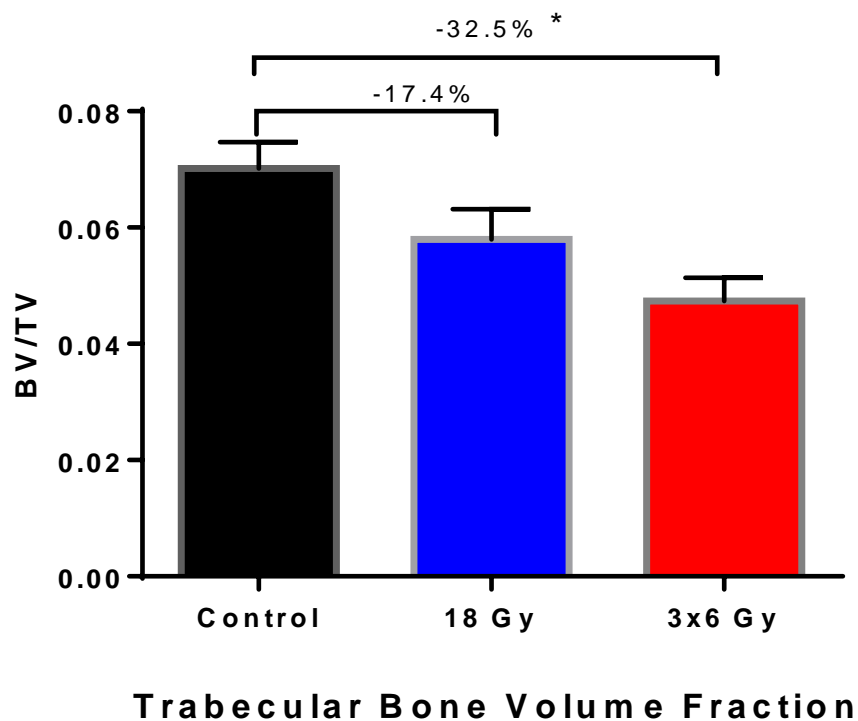

Figure 8: Trabecular bone volume fraction (BV/TV) indicates the fraction of a given volume of interest that is occupied by mineralized bone The fractionated group show significant bone loss compared to the control. Although sizable, the acute dose group's decrease in BV/TV compared to the control was not deemed statistically significant. Mean +/- SEM.

$*P < 0.05$

Volumetric Bone Mineral Density

Figure 9 shows the results for the volumetric bone mineral density (vBMD). This follows a similar trend to BV/TV, with both irradiated groups showing notable decrease when compared to the control. The 18 Gy group showed a decrease of 31.9% compared to the control (p-value = 0.0239). The 3x6 Gy fractionated group showed a 57.4% decrease when compared to the control (p-value < 0.0001). The differences for both the single acute dose and fractionated groups are deemed statistically significant.

Like BV/TV, there is also a noticeable difference between the 18 Gy and 3x6 Gy irradiated groups. Again, it was not deemed statistically significant, with a p-value of 0.0831.
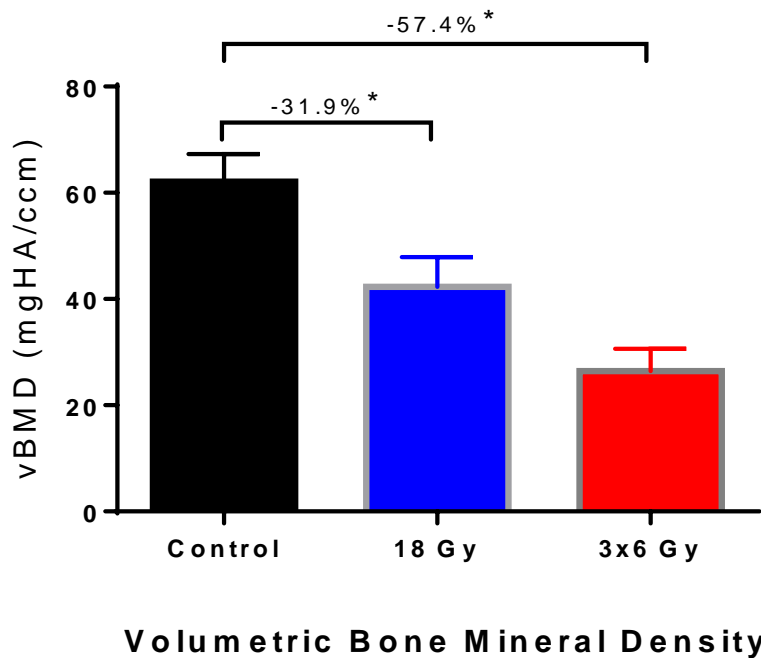

Figure 9: Volumetric bone mineral density (vBMD) indicates the average bone mineral density in a given volume of interest. Both fractionated and acute dose groups showed statistically significant loss in vBMD compared to the control. Mean +/- SEM. *P < 0.05

Connectivity Density

Results for connectivity density (ConnD) are shown below in Figure 10. The data follow the general trend as seen so far, with both irradiated groups showing decreased values when compared to the control. However, the differences were not deemed statistically significant. The 18 Gy group showed a 19.6% decrease (p-value = 0.6384), while the 3x6 Gy group showed a 40.5% decrease (p-value = 0.1598). The difference between the two irradiated groups was also not statistically significant.
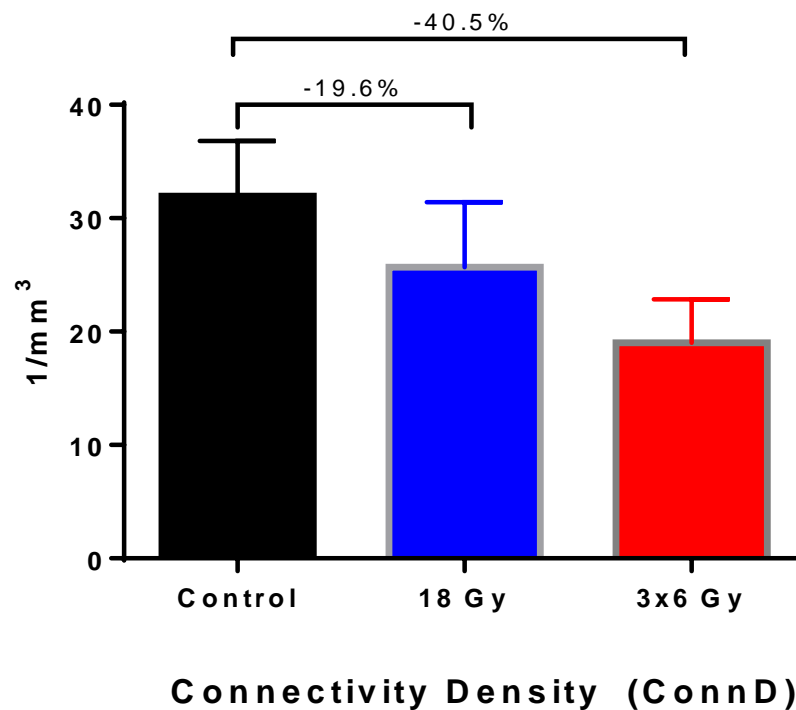

Figure 10: Connectivity density (ConnD) measures the degree of connectivity of trabeculae normalized by total volume. Both irradiation groups show sizable decreases compared to the control, but the differences were not deemed statistically significant. Mean +/- SEM.

$*P < 0.05$

Trabecular Number

   The trabecular number (TbN) shows statistically significant differences in both the 18 Gy and 3x6 Gy groups when compared to the control. The 18 Gy group exhibited a 12.6% decrease (p-value = 0.0410), while the fractionated group showed a bigger 19.6% drop (p-value = 0.0011). The difference between the 18 Gy single dose and the 3x6 Gy fractionated group was not deemed statistically significant.
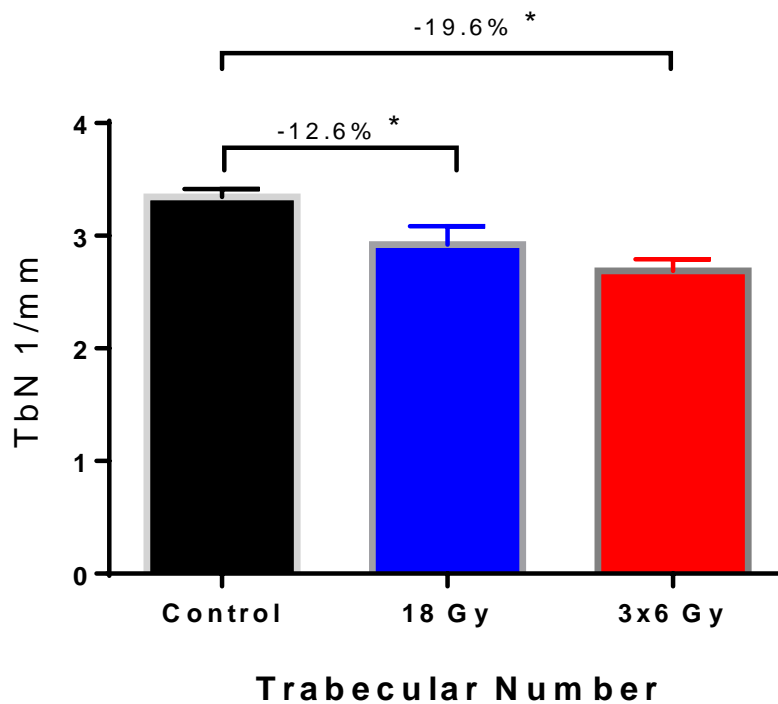

Figure 11: Trabecular number (TbN) measures the average number of trabeculae per unit length. Both the single acute and fractionated groups show statistically significant decrease compared to the control. Mean +/- SEM. *P < 0.05

Trabecular Thickness

The trabecular thickness (TbTh) results are shown below in Figure 12. There is minimal difference among all three groups. No statistically significant results were observed.
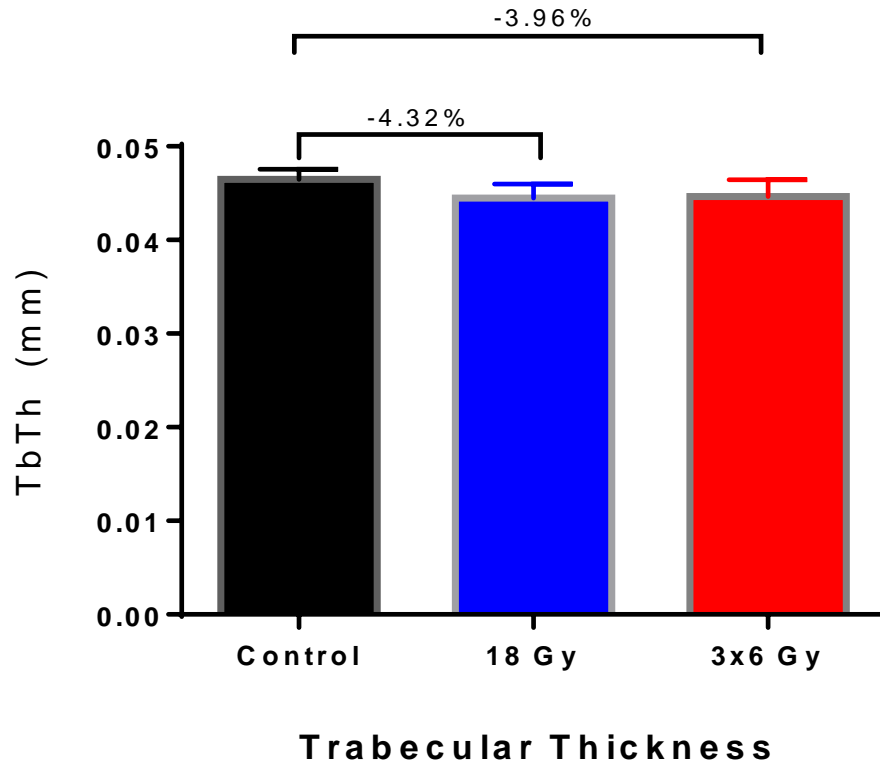

Figure 12: Trabecular Thickness (TbTh) indicates the mean thickness of trabeculae. No statistically significant differences were observed among all three groups. Mean +/- SEM. *P < 0.05

Trabecular Separation

Trabecular separation (TbSp) results are shown below in Figure 13. Again, there are differences between the irradiated groups and control, and they are both statistically significant. The 18 Gy single dose group showed a 17.7% increase in trabecular separation (p-value = 0.0414). The 3x6 Gy fractioned group showed an even bigger 27.1% increase (p-value = 0.0013). The difference between the 18 Gy and 3x6 Gy fractionated group was again not statistically significant.
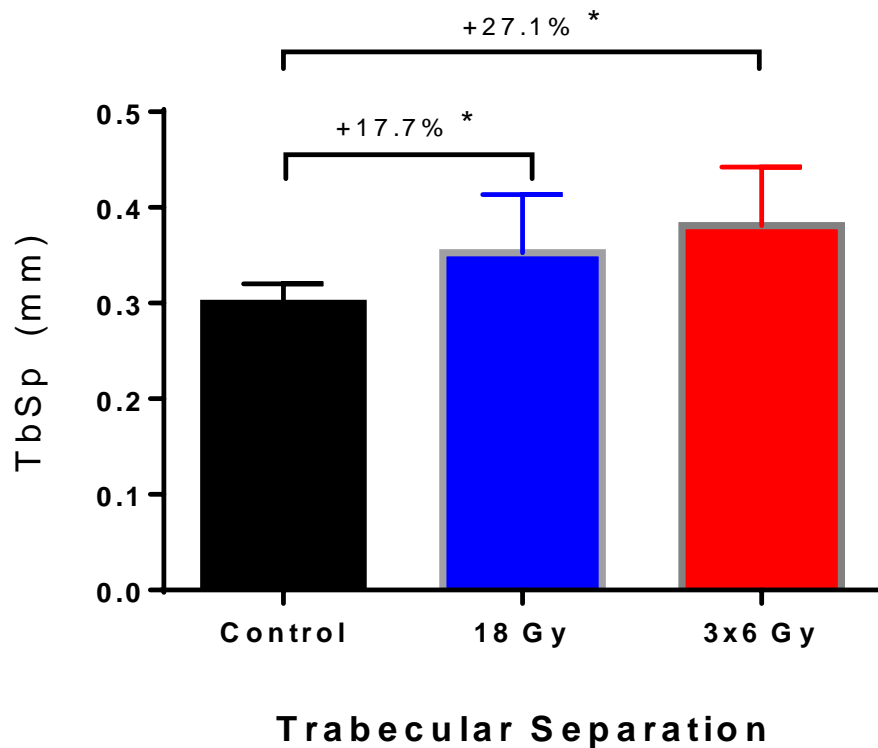

Figure 13: Trabecular separation (TbSp) indicates the mean distance between trabeculae. Both irradiated groups show statistically significant increase in TbSp compared to the control, with the fractionated group showing notably more increase than the acute dose group. Mean +/- SEM. *P < 0.05

Micro-CT – Qualitative Analysis

Data obtained from the SCANCO μ80 micro-CT scanner were used to generate subject specific finite element models in Abaqus. The following figure depicts examples of the raw micro-CT images, showing the metaphysis region of interest from each of the three study groups. The visual differences in the trabecular bone between the groups are noticeable, with the changes in trabecular number, thickness and spacing most apparent.
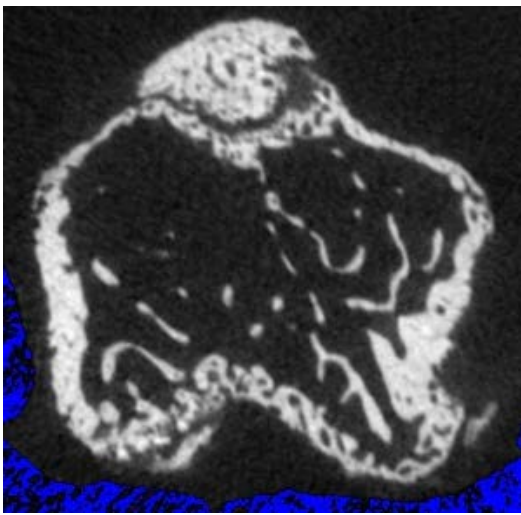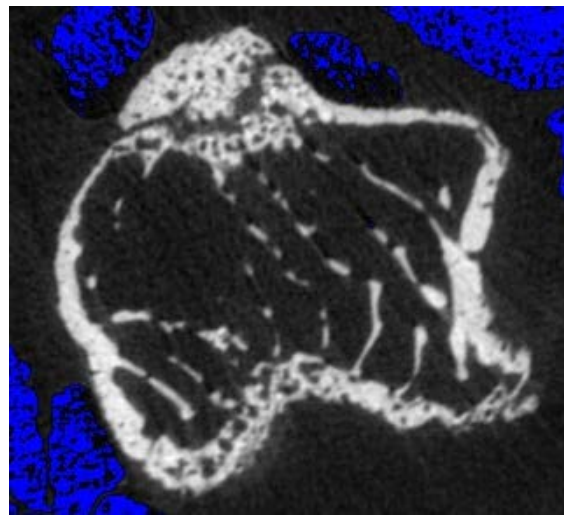
(a) 18 Gy acute dose   (b) 3x6 Gy fractionated
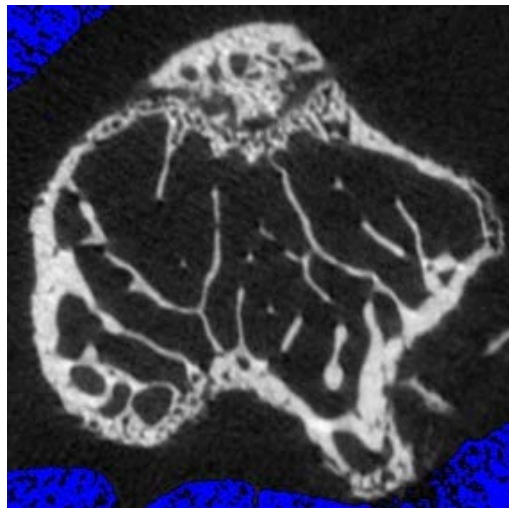
(c) non-irradiated

Figure 14: Micro-CT images from all three groups. Note the differences in trabeculae quality.

The segmented trabecular bone micro-CT images from the same specimens in the previous figure are depicted below. Visually, there appears to be a reduction in connectivity and volume in both of the irradiated groups compared to the control, with the 3x6 specimen showed the most pronounced loss.
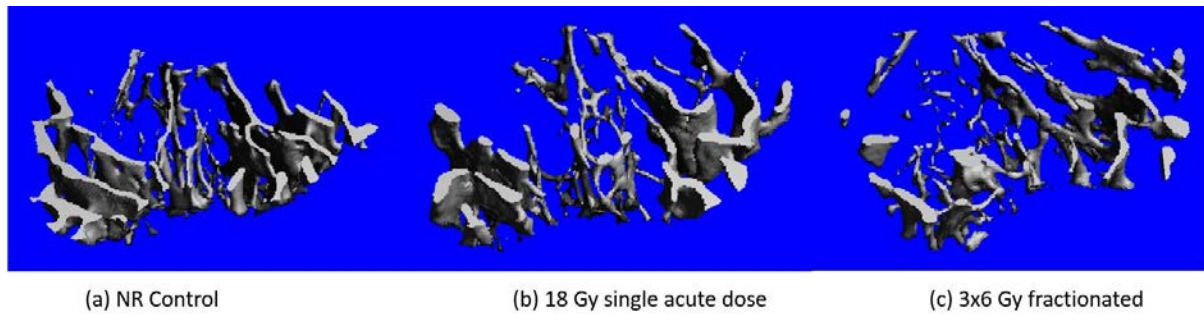

(a) NR Control   (b) 18 Gy single acute dose   (c) 3x6 Gy fractionated

Figure 15: Isolated trabecular struts from all three groups. Note the visual changes in trabecular connectivity, number and separation.

Finite Element Analysis – Compression Test

Once the subject specific model was generated for each specimen in Abaqus, the basic compression test was performed by creating a fixed boundary condition at the most distal surface of each model. Figure 16 highlights the bottom plane in red.
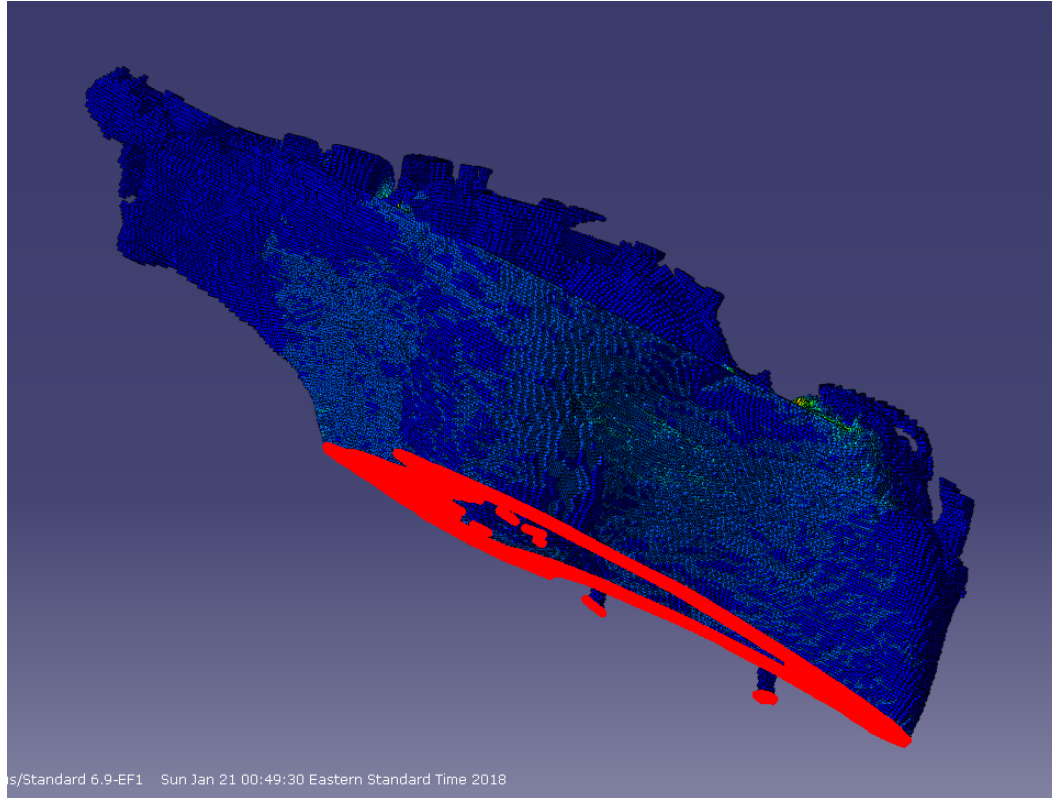
Figure 16: Side view of 18 Gy specimen 3052 under load, whole bone

The same specimen is illustrated in figures 17-18 from different perspectives, with and without the trabecular struts inside the cortical shell. The color distribution throughout the model gives a visual interpretation of the level of load each region is experiencing. The legend in the top left corner shows how the stress level ranges from low (blue) to green (medium) to high (red). Figure 19 shows another specimen from the 3x6 Gy fractionated group in unloaded and loaded condition.
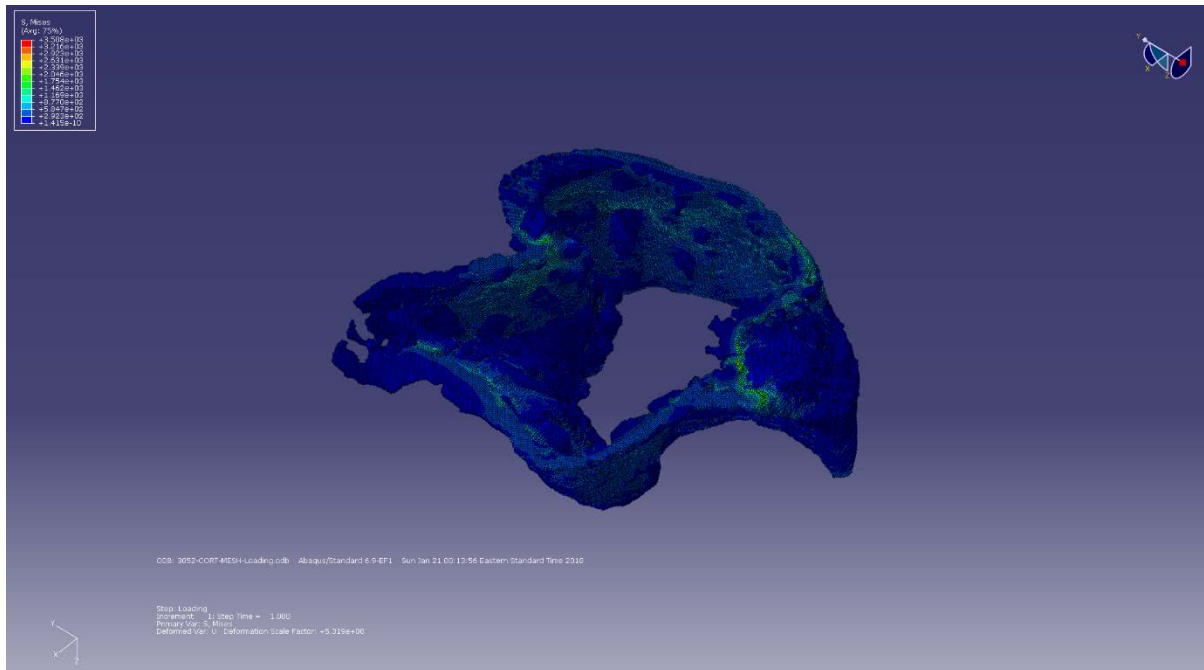
Figure 17: Under load, 18 Gy specimen 3052, cortical only
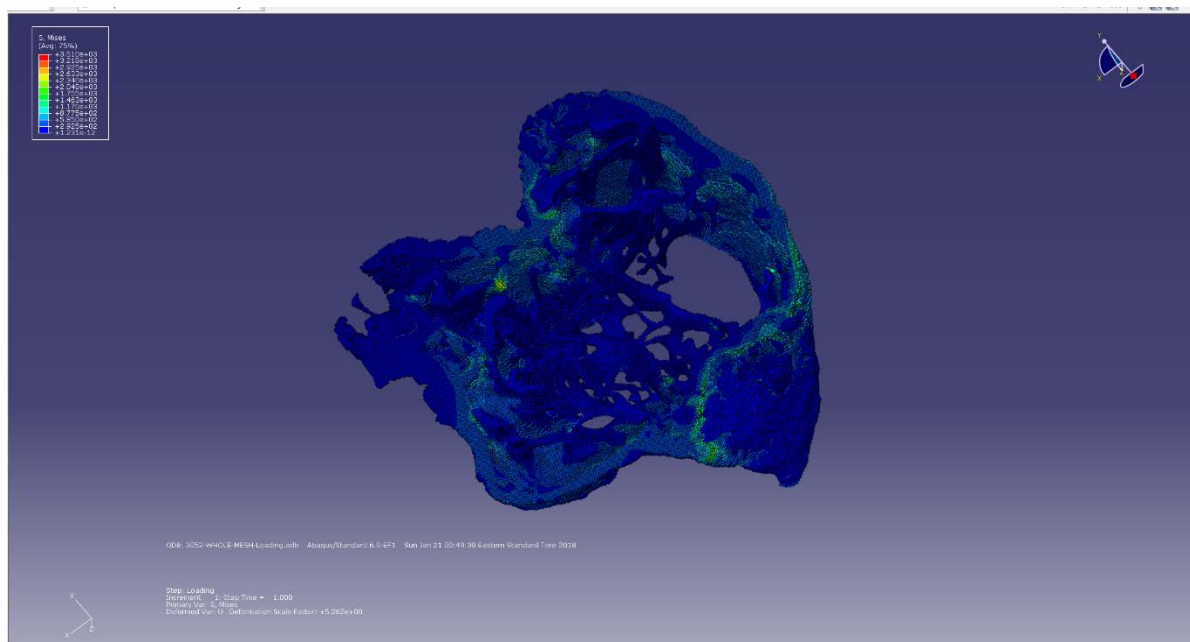
Figure 18: Under load, 18 Gy specimen 3052, whole bone
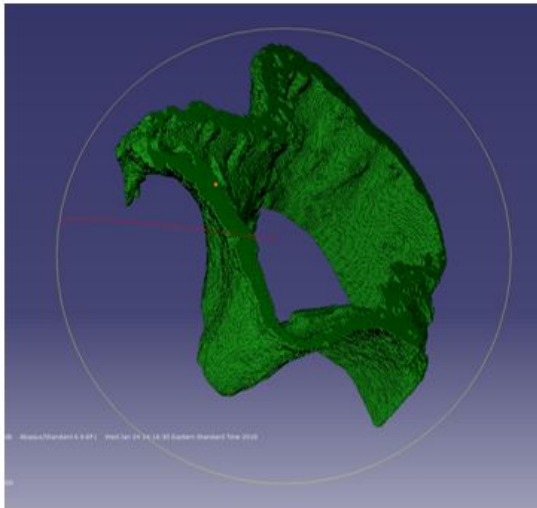
(a) Cortical only, unloaded
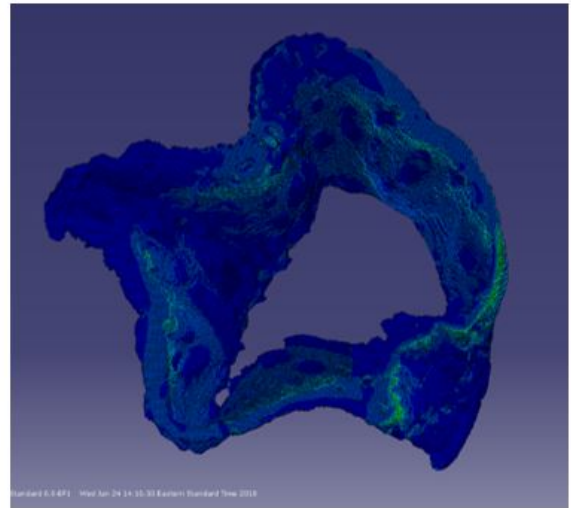
(b) Cortical only, under 5% compressive load
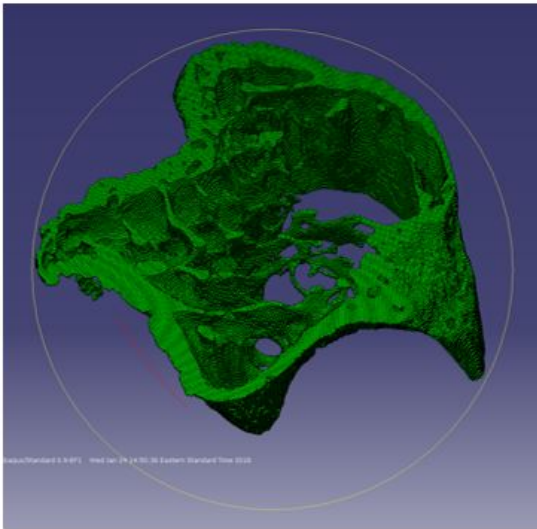
(c) Whole bone, unloaded
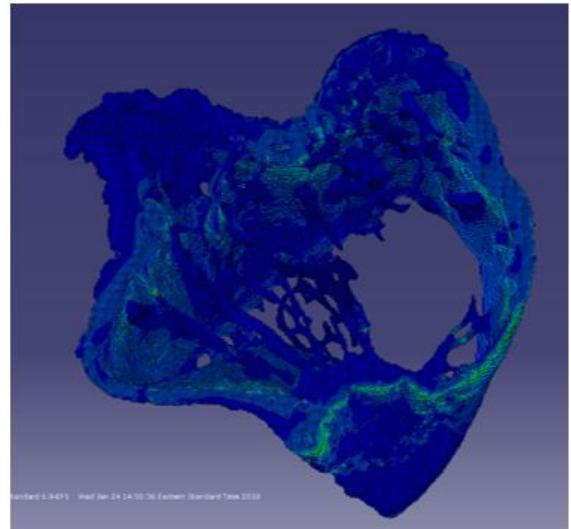
(d) Whole bone, under 5% compressive load

Figure 19: 3x6 Gy specimen, cortical and whole bone, with and without loading

The mean summation of force results from the FE compression test are shown in the following figures. Figure 20 shows results from testing only the cortical bone, while figure 21 shows results from testing the entire bone complex, including the trabecular bone. There were minimal differences and no statistically significant results across all groups.
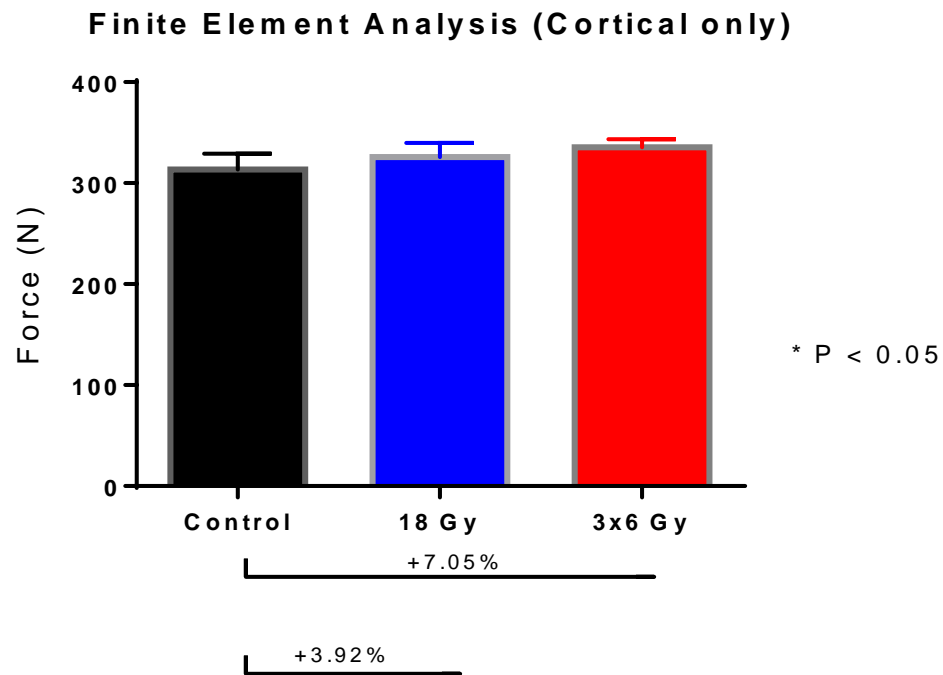
Figure 20: FEA (cortical bone only). No significant differences. Mean +/- SEM. *P < 0.05
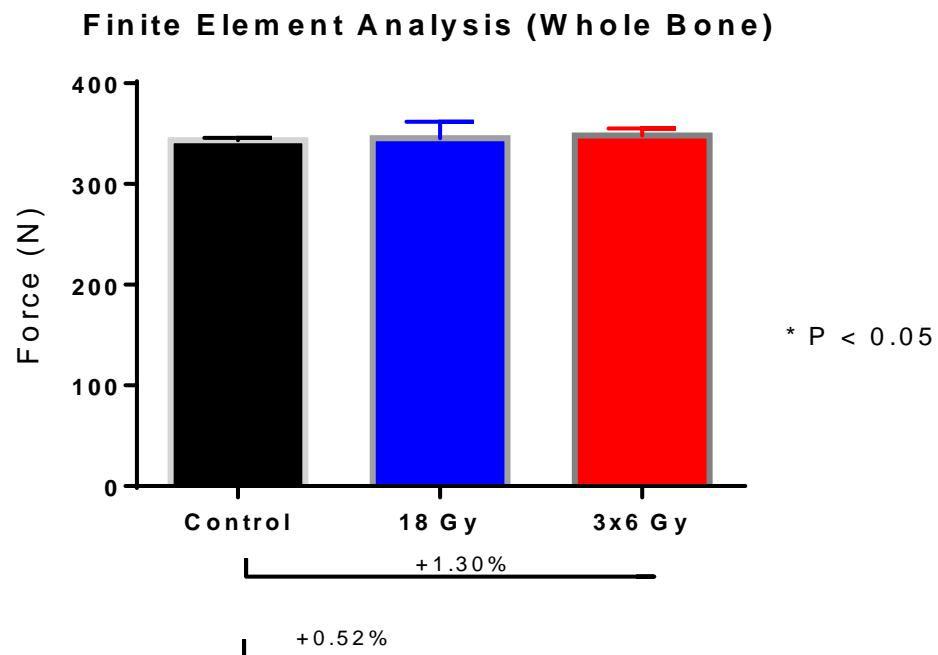
Figure 21: FEA (whole bone). No significant differences. Mean +/- SEM. *P < 0.05
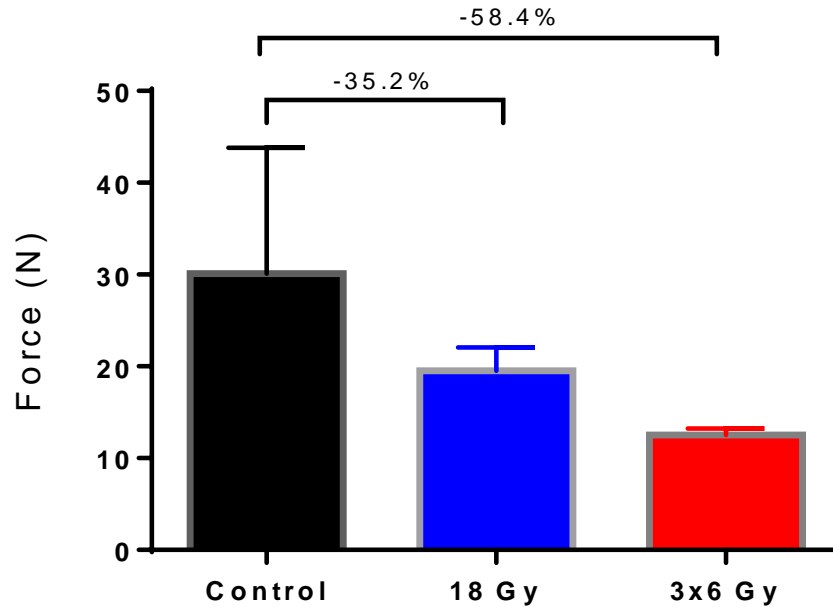
Figure 22: FEA (trabecular only). Even though sizable differences were observed between the irradiated groups and the control, they were deemed not statistically significant. Mean +/- SEM. *$P < 0.05$

The result from trabecular only analysis is shown in figure 22. Despite the notable decrease between the irradiated groups and the control, with the 18 Gy group showing -35.2% and 3x6 Gy fractionated group showing -58.4%, those differences were deemed to be not statistically significant. By comparing with figures 21-22, the relative contribution of trabecular bone can be seen at slightly less than 10% in the control group, and decreasing further in the irradiated groups. In addition, the error bars seem to suggest an interesting trend in decreasing variance from the control to the single acute dose followed by the fractionated dose group.

Stiffness

The stiffness values for the cortical bone and whole bone are shown in figures 23 and 24, respectively. There were no statistically significant differences among the study groups.
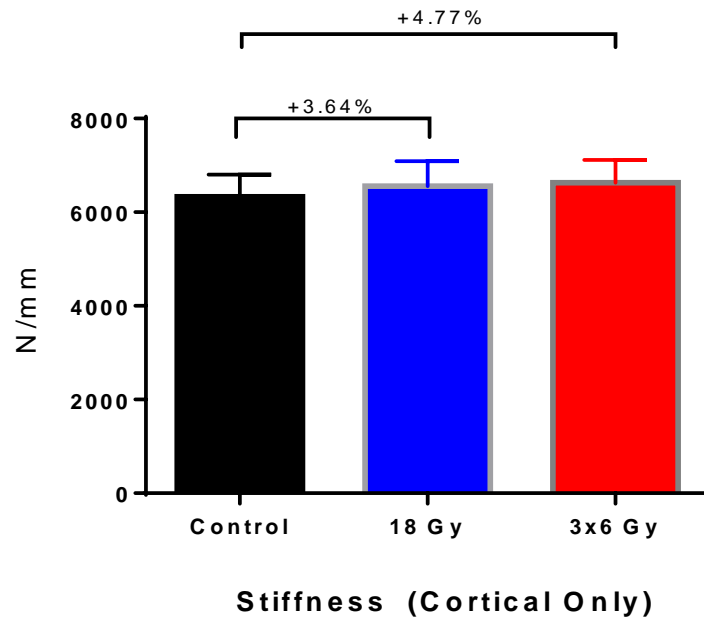
Figure 23: Stiffness, cortical bone only. Mean +/- SEM. *P < 0.05

Figure 24: Stiffness, whole bone. Mean +/- SEM. *P < 0.05

The stiffness values for the trabecular bone showed a different trend. Both irradiated groups showed statistically significant loss in trabecular stiffness compared to the control. The 18 Gy single acute dose group showed a 20.5% loss (P=0.04), while the 3x6 Gy fractionated dose group exhibited a 39.3% loss (P<0.0001). Comparisons between the 18 Gy and 3x6 Gy fractionated groups did not show a statistically significant difference.
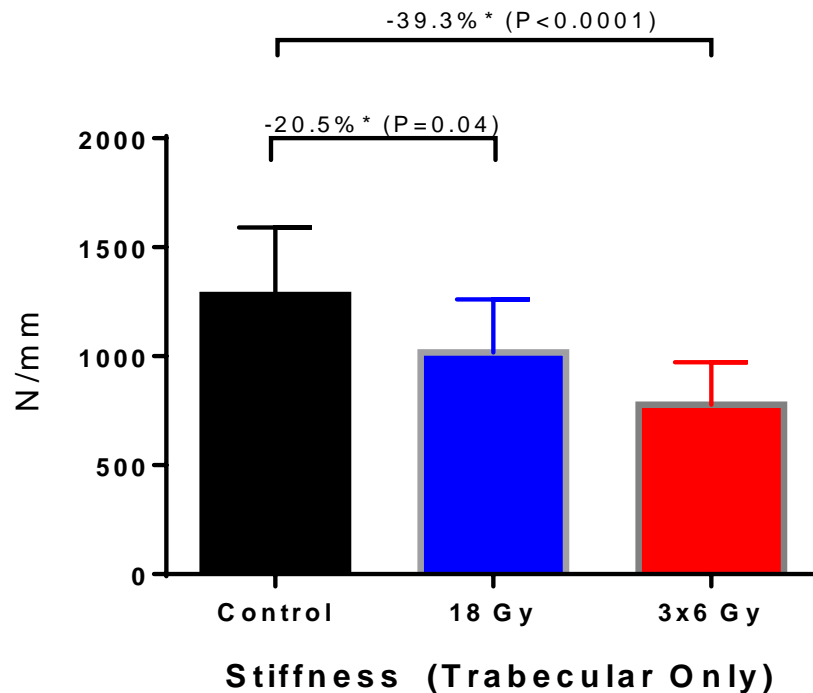
Figure 25: Stiffness, trabecular only. Both irradiated groups showed statistically significant loss in trabecular stiffness compared to the control. Mean +/- SEM. *P < 0.05

Structural Efficiency

The mean structural efficiency results (stiffness divided by the bone volume) for the cortical bone alone and the whole bone are shown in figures 26 and 27, respectively. As with the basic compression test seen earlier, there were minimal differences between the groups, and none of the differences were statistically significant.
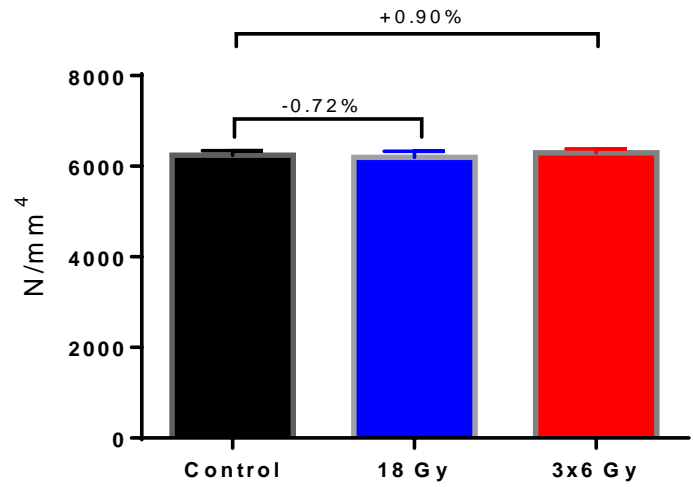
Structural Efficiency, Cortical Only

Figure 26: Structural efficiency, cortical bone only. No statistically significant differences were observed. Mean +/- SEM. *P < 0.05
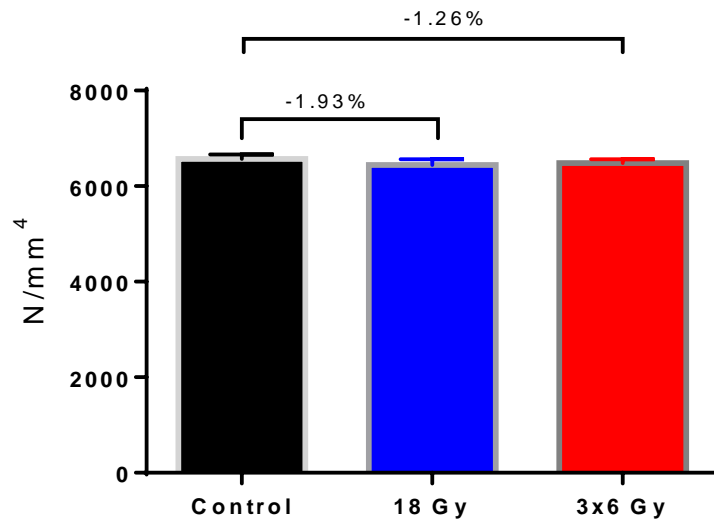
Structural Efficiency, Whole Bone

Figure 27: Structural efficiency, whole bone. No statistically significant results were observed. Mean +/- SEM. *P < 0.05

The structural efficiency result for the trabecular bone showed a different trend. The

3x6 Gy fractionated dose group showed a statistically significant 42.5% decrease in

structural efficiency compared to the control group (P=0.0021). The 18 Gy single acute dose

group also showed a sizable decrease, however the difference was not deemed statistically

significant. No statistically significant differences were observed between the two irradiated
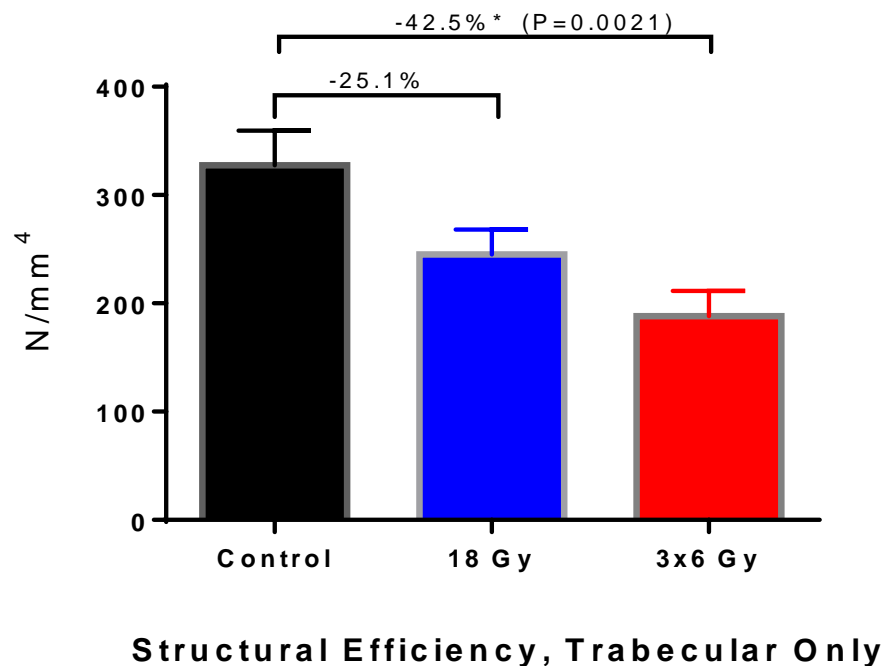
groups.

Figure 28: Structural efficiency, trabecular only. The 3x6 Gy fractionated group showed
statistically significant 42.5% decrease compared to the control. The 18 Gy single acute dose
group also showed a sizable decrease compared to the control, but this difference was not
statistically significant. No significant differences were observed between the two irradiated
groups. Mean +/- SEM. *P < 0.05

CHAPTER 4: DISCUSSION AND FUTURE WORK

The results from this study indicated that although the two irradiated groups clearly suffered some level of bone loss, it was not as pronounced as anticipated. In addition, none of the results pointed to a statistically significant difference in the degree of bone loss between the single acute dose and fractioned group. These findings do not support our hypothesis that a large single acute dose would be more damaging than its fractionated counterpart.

Body Weight

The average mice weight data shown in figure 7 shows an expected trend. All three groups started with similar body mass and exhibited a decrease in the early days of the study. This could be attributed to stress induced by a new environment and handlers. Both irradiated groups showed a sharper decline in weight than the control. This was expected, as the side effects of radiation exposure such as nausea and fatigue may have played a role. Of note, the 18 Gy group quickly recovered by the midpoint of the study and mirrored the control group from that point on, while the 3x6 Gy group did not recover as quickly or robustly. This was most likely due to the repeated radiation exposure and the accompanying periods of distress.

Trabecular Microarchitectural Parameters

The various trabecular microarchitectural parameters obtained from the micro-CT analysis showed a clear trend at first glance. Trabecular bone volume fraction (BV/TV), volumetric bone mineral density (vBMD), trabecular number (TbN) and separation (TbSp) all indicated statistically significant bone loss in the two irradiated groups relative to controls.

Similar effects of ionizing radiation on healthy bone tissues has been established in literature, and these findings were within expectations and comparable with previously establish works (Hamilton et al., 2006; Willey et al., 2011; Willey et al., 2008; Wright et al., 2015).

There was no clear relationship between the 18 Gy single acute dose and 3x6 Gy fractionated group. We had hypothesized that the acute dose would be more traumatic and result in more pronounced bone loss compared to fractionation, and there was no statistically significant evidence for or against it here. However, the dataset overall does follow a general trend of the fractionated group consistently performing poorer than the 18 Gy group across the six trabecular parameters examined. For example, ConnD, while deemed not statistically significant, declined in both irradiated groups compared to the control, with the 3x6 Gy group showing roughly double the loss as the 18 Gy group. With BV/TV and vBMD, the 3x6 Gy group consistently exhibited close to double the amount of percentage loss vs control when compared with the 18 Gy group. Trabecular number and separation also continued this trend, with the 3x6 Gy group showing at least 50% more percentage difference versus control when compared with the 18 Gy group. With the trabecular thickness results showing very little difference between the two irradiated groups, the trabecular parameters as a group suggest a more complicated relationship than originally anticipated between the single acute and fractionated dose groups.

Finite Element Analysis

The motivation for pursuing finite element analysis was to gain additional insight into the effect of the structural changes induced by radiation on bone strength. One way to characterize bone strength is through its stiffness, which is defined as the force divided by displacement produced by the force, or $k=F/\delta$. Structural efficiency, defined as stiffness

divided by total bone volume, can provide an additional method of characterizing and quantifying the effect of changes in the bone's overall strength.

For the scope of this study, we assumed the bone to be isotropic in nature. The material properties were assigned an elastic modulus of 10 GPa and Poisson's ratio of 0.3, which are the classically accepted values in this research area and experimentally verified (Blanchard et al., 2013; Chattah et al., 2009; Nyman et al., 2015). This allowed us to perform the axial compression test with our subject specific finite element models and obtain a preliminary understanding of the overall effect on bone strength from changes in the bone's structural integrity. In doing so, we need to be mindful of the limitations imposed by this assumption in material property. By assigning the same material property values to both trabecular and cortical bone, we are assuming the entire bone to be completely homogeneous. As a result, our FE model is examining only the structural component and does not take into account any variability in material properties. At first glance, this might make our data highly sensitive to variations in the elastic modulus. However, since we are using a linear elastic model, we would not see any difference in the data as the results would all scale accordingly as long as there is no structural change. In addition, we can ascertain the roles played by the cortical and trabecular bone, and consequently their effect on overall bone strength, by looking at their relative strength compared to one another. Indeed, this was the motivation for examining our FEA models in whole bone and cortical/trabecular only configurations.

Analysis on the trabecular only configuration revealed some interesting results. Even though they were deemed not statistically significant, the summation of forces results shown in figure 22 hinted at a decreasing trend in trabecular strength from the control to the two irradiated groups. In addition, the variability observed in the three study groups showed a

remarkable trend of decrease. The control group exhibited notable variance, but this variability was vastly reduced in the 18 Gy single dose group and virtually disappeared in the 3x6 Gy fractionated dose group. The trabecular stiffness result shown in figure 25 also supported the trend of decreasing trabecular strength, with the 18 Gy group showing 20.5% loss (P=0.04) and the 3x6 fractionated group showing close to twice as much loss at 39.3% (P<0.0001) compared to the control. Structural efficiency results followed a similar trend, with the 3x6 Gy fractionated dose group showing a significant decrease of 42.5% (P=0.0021) compared to the control. Together, these results suggested a significant decrease in overall trabecular strength post radiation, with the 3x6 Gy fractionated dose group suffering notably greater loss than the 18 Gy single acute dose group. Furthermore, the trend of decreasing variability observed in the summation of forces results was very interesting. It hinted at trabecular bone's radiosensitivity, suggesting that fractionation may have caused more rapid and uniform loss in trabecular strength.

The FEA results for whole bone and cortical only showed no statistically significant differences. This lack of change in overall bone strength post radiation suggested that despite notable degree of trabecular bone loss from irradiation, the overall strength of the tibia was not significantly impacted in a negative manner. This could be clearly observed in our FEA mean summation of force result shown in figures 20-22. While the changes observed were not deemed statistically significant, the relative contribution of the trabecular bone was lower than 10% of the total bone strength in the control group, and even lower in the two irradiated groups. In other words, our FEA results seemed to suggest that trabecular microstructural changes do not play significant roles in the overall bone strength. This in term presented a potential discordance with the clinical evidence of increased prevalence of hip fracture in

gynecological cancer patients receiving radiotherapy. One plausible explanation is that the bone, being a dynamic system, is able to sufficiently compensate for the loss in trabecular structural strength through other means, at least in the early stages. In their 2010 study, Wernle et al investigated the effect of local irradiation (5 or 20 Gy) on the bone strength of 13 week-old female Balb/c mice. By looking at time points 2, 6, 12 and 26 weeks after irradiation, Wernle et al found that the mice actually exhibited an increase in bone volume and strength at 2 weeks post irradiation. By week 12, there was a loss of bone strength despite the higher bone volume (Wernle et al., 2010). Their result was indicative of a decrease in overall structural efficiency and possibly a change in the bone material property. With our study, we observed significant trabecular bone loss but did not observe any statistically significant changes in overall structural efficiency and bone stiffness. While the results from the Wernle study may not be directly comparable due to the differences in study design (irradiation dosage, mice strain and study length), they point to the possibility that a similar effect of bone strength fluctuation in the early stages post irradiation may be in play in our study, which may have contributed to the observed FEA results. Despite some differences in study design, both studies point to the importance and significance of material property change in bone strength. It is plausible that changes in material property play a bigger role than structural changes in overall bone strength than previously anticipated. From a clinical perspective, this could help to explain the higher incidence of fracture post radiotherapy observed in cancer patients.

Another reason for the discordance between the clinical data of fracture incidence rate in gynecological patients and our FEA results could be the inherent limitations of our FE model. As pointed out earlier, we assumed the material property of the bone to be isotropic

and homogeneous. Consequently, we assumed the material model to be linear elastic and the small displacement performed in the axial compression test to be within this linear region. This meant our FE model was a good model throughout the linear elastic region of the bone's stress-strain curve, but it provided no information about the actual failure point. This was sufficient for this study, as the focus was on the effect of changes in radiation-induced structural changes in the bone and their effect on overall bone strength. In order to get a more complete picture that includes information on yield point and material properties, further work would be required. This could be achieved experimentally with nano-indentation to refine the model (Blanchard et al., 2013; Nyman et al., 2015).

In summary, structural strength characterized through stiffness and structural efficiency provided an incomplete picture of overall bone strength. The assumptions made regarding the bone's material property limited the validity of our FE model to the linear elastic portion of the stress-strain curve. While micro-CT and our specimen-specific FE models allowed for a detailed look into changes in trabecular structure, it did not provide information on its material property or failure point. Even though the differences in stiffness and structural efficiency were all deemed statistically insignificant, together they seem to hint at a potentially interesting development – a compensation mechanism where the cortical bone somehow increases its stiffness to compensate for the loss in trabecular structural strength. There are many factors that affect cortical bone's mechanical competency, including bone mineral density, bone mineral content, cortical thickness, cortical porosity and crystallinity (Augat and Schorlemmer, 2006). It is plausible that the cortical shell underwent changes in some or all of the above mentioned parameters as a response to losses in trabecular strength.

Even though it was beyond the scope of this manuscript, the effect of potential compensation mechanisms certainly presents a logical next target for future studies.

Sources of Variance

In their 2016 study, Crezee et al found that hyperthermia combined with radiotherapy significantly improved regional control and overall survival for cervical tumors compared to radiotherapy alone (Crezee et al., 2016). Of course, this clinical human study cannot be directly compared to our preclinical animal model. In addition, the targets in the Crezee study were cervical cancer cells, which have altered metabolism and radiation response compared to normal, healthy cells. Indeed, we must recognize that the radiation treatments used in the mouse are often quite different than their human counterparts (Verhaegen et al., 2011). Still, these findings suggest that temperature could be another factor that affects biologic tissue radiosensitivity.

Another potential source of variance is the immobilization procedures used to secure the mice for irradiation. In general, cells with high radiosensitivity or early responding behaviors to radiation have a higher alpha/beta ratio than those with lower radiosensitivity (Douglas and Fowler, 1976; Fowler, 2010; Williams et al., 1985). In their 1993 study, Stuben et al examined the effect of different immobilization procedures on single dose and fractionated dose irradiation. They found that the effect of different immobilization procedures changed the alpha/beta ratio in Foster's equation, especially when large fraction sizes are involved (Stuben et al., 1993). Further look into this effect of immobilization procedures on radiosensitivity could help reduce the amount of type I errors in the characterization of radiation-induced bone loss.

A recurring theme in our data was the presence of observed trends in some parameters that lacked statistically significant differences. For example, the trabecular parameter ConnD (connectivity density) showed a notable decrease in both irradiated groups compared to the control. The 18 Gy group declined 19.6%, while the 3x6 Gy group lost just over twice as much at 40.5% compared to the control. Both differences were not statistically significant. Another example would be the trend of the 3x6 Gy fractionated group consistently showing more negative results across the parameters when compared to the 18 Gy single acute dose group, but without statistically significant differences. One possible explanation could be attributed to the innate nuisances of the trabecular parameters. For instance, the trabecular thickness (Tb.Th) parameter by definition was a scalar mean for the given region of interest (ROI). While it could be a good indicator for the overall thickness and health of the trabeculae, Tb.Th's nature as an average meant that it had the potential to overlook some structural changes. Hypothetically, two groups can have the same Tb.Th values even if they contained radically different trabecular architecture. One group could contain trabeculae with uniform thickness, while the other could contain thick trabeculae interconnected by thin struts.

Another possible reason may be attributed to the micro-CT analysis process. Once specimen was scanned, the cortical and trabecular sections were manually delineated through the creation of contours or regions of interest. This process certainly had the potential to introduce extra variance in the border region between the two sections. We were mindful of this potential source of variance and planned the study accordingly to minimize its impact. The same person traced all samples in the study to maintain consistency in the creation of the cortical and trabecular sections. Auto-contouring, used across all specimen samples, further

reduce potential variance by minimizing manual tracing and maximizing consistency. Another potential source of variance in the micro-CT analysis process was segmentation, or the identification of bone material in the region of interest. A threshold value for mineralized material was used to accept or reject a voxel as bone material, ideally including all visible bone while excluding all other artifacts. This is an inherently imperfect system for a couple of reasons. First, since newly formed osteoid has lower density than older bone, some might not be identified correctly depending on the age of the bone tissue. Second, it is plausible that there might be some variation in the rate of mineralization among individual animals, which might lead to additional variances across the study groups. To minimize variances from the segmentation process, we drew upon our research lab's significant past experience and study results in choosing the optimal threshold value. In addition, the homogeneity of the mice age and normalization of their weight across study groups would have helped to mitigate variance from differences in the rate of mineralization among the animals. Finally, the SCANCO micro-CT scanner automatically applies a Gaussian filter on the raw image for noise reduction purposes. Even though it is an established process and does a good job in reducing noise, the filter is not perfect and will inevitably allow some noise to get through. The presence of this noise could potentially introduce some error in the segmentation process and parameter calculations.

Even though our sample size of twelve mice per study group was reasonable and no animals were lost or excluded prematurely, we cannot rule out that a higher statistical power may have been helpful to counter the seemingly higher than expected variance (Charan and Kantharia, 2013). For future studies, it would be beneficial to have broader collaboration with additional experts in biostatistics to ensure adequate statistical power.

Mouse Model Limitations

The choice of the C57BL/6 mouse as the animal model for this study was based on the similarities in skeletal system and bone remodeling process between the strain and its human counterpart. It has been argued that by using a single inbred strain, such as the C57BL/6, studies may potentially generate results that is not entirely applicable to the population at large since it might have been dependent upon the unique collection of genes in an inbred strain (Miller et al., 1999). A counterargument suggests that genetically heterogeneous mice represent a poor source material for controlled studies due to the inherent phenotypic variability and resulting decline in experimental sensitivity (Festing, 1999). There are valid points on both sides of the aisle.

In the context of this study, the C57BL/6 mouse strain fulfills the needs of our animal model with great proficiency. As with humans, C57BL/6 mice start to lose cancellous or trabecular bone early in adulthood (Halloran et al., 2002). Both also start to experience loss of bone strength before loss of BMD determined via DXA (Almeida et al., 2007; Hui et al., 1988). The median life span of this strain is 901 days for males and 866 days for females (Yuan et al., 2009). This relatively long life span pushes unwanted age-related pathologies, metabolic disorders and illnesses further back compared to mouse strains with shorter life spans, thus reducing the chance of their involvement in any observed changes in bone structure or bone loss (Jilka, 2013).

Of course, no animal model is completely perfect. In humans, age-related changes in trabecular architecture involve decreased trabecular connectivity, number and thickness, with a larger decrease in thickness in men than in women (Seeman, 2002). C57BL/6 mice only shows decline in trabecular connectivity and number but not thickness (Glatt et al., 2007).

Possible causes for this difference may be the much higher bone turnover rate and smaller scale of the mouse skeleton, where thinned trabecular bones are more transient and less likely to be observed (Jilka, 2013). Another notable difference between mice and humans is that mice do not undergo a true menopause. Instead, they exhibit irregular cycling, typically around 8 to 12 months of age in the case of the C57BL/6 mice (Mobbs et al., 1985). Still, the fact that the C57BL/6 strain is used extensively in the field of age-related bone loss and osteoporosis means there is a wealth of knowledge on this particular strain from previous studies. This adds to the robustness of the animal model as it makes it easier to compare data and build upon previous work.

Future work

The results from this study compared well with established knowledge regarding basic bone loss induced by radiation compared to a non-irradiated control group. The relationship between single acute dose and the equivalent fractionated dose group was not as clear. As we mentioned before, the skeletal system is complex and dynamic. It is very plausible, and highly likely, that there are still many confounding factors that may not be obvious or sensitive to micro-CT and FEA by themselves. As we pointed out earlier, the primary limitation in our FEA model was the assumption made with the material properties of the bone. The resulting model was sufficient for the linear elastic region of the bone's stress-strain curve, but it provided no information about the actual failure point. Overall bone strength depends not only on structural integrity but also material property as well. For example, Wernle et al showed in their 2010 study a decrease in bone strength despite an increase in bone volume post irradiation. This result strongly pointed to a causal relationship between loss of bone strength and changes in material properties. Therefore, the logical next

step from this study would be to take a deeper look at bone material property. Experimental tests such as micro and nano-indentation would help provide crucial material property information that could be used to refine our FE models. To investigate other potential confounding factors, examination of the bone on the cellular level would be another promising path, starting with incorporating histological analyses such as hematoxylin and eosin staining, an established method for studying morphologic changes in cells and tissues (Fischer et al., 2008). The various signaling pathways and biomarkers associated with the bone remodeling cycle would be another area of future research that could provide new insights. Interdisciplinary collaboration with other experts in pathology, histology and molecular biology should be pursued to allow for an even more comprehensive investigation approach.

Future studies may also want to explore adding more variation in radiation dosage. This could help reveal more information and improve upon the dose-response relationship. Longitudinal studies using additional techniques such as quantitative computed tomography could be useful in revealing more information about ionizing radiation's long term effect on cell recovery and repair process, ultimately aiding in clinical treatment refinement.

REFERENCES

Aarden, E.M., Burger, E.H. and Nijweide, P.J., 1994. Function of osteocytes in bone. J Cell Biochem. 55, 287-99.

Ackert-Bicknell C, B.W., Rosen CJ, Sundberg JP. Aging Study: Bone Mineral Density and Body Composition of 32 Inbred Strains of Mice., MPD;Ackert1. The Jackson Laboratory, Bar Harbor, ME.

ACS, 2017. Cancer Facts & Figures 2017. American Cancer Society.

Allen, M.R. and Burr, D.B., 2014. Basic and applied bone biology, Academic Press, London; Waltham, MA.

Almeida, M., Han, L., Martin-Millan, M., Plotkin, L.I., Stewart, S.A., Roberson, P.K., Kousteni, S., O'Brien, C.A., Bellido, T., Parfitt, A.M., Weinstein, R.S., Jilka, R.L. and Manolagas, S.C., 2007. Skeletal involution by age-associated oxidative stress and its acceleration by loss of sex steroids. J Biol Chem. 282, 27285-97.

Augat, P. and Schorlemmer, S., 2006. The role of cortical bone and its microstructure in bone strength. Age Ageing. 35 Suppl 2, ii27-ii31.

Baxter, N.N., Habermann, E.B., Tepper, J.E., Durham, S.B. and Virnig, B.A., 2005. Risk of pelvic fractures in older women following pelvic irradiation. JAMA. 294, 2587-93.

Bellido, T., Plotkin, L., Bruzzaniti, A, 2014. Basic and Applied Bone Biology, Elsevier, San Diego, CA.

Beyzadeoglu, M.O., G; Ebruli, C, 2010. Basic Radiation Oncology, 1 ed. Springer-Verlag Berlin Heidelberg.

Blanchard, R., Dejaco, A., Bongaers, E. and Hellmich, C., 2013. Intravoxel bone micromechanics for microCT-based finite element simulations. J Biomech. 46, 2710-21.

Burr, D.B. and Akkus, O., 2014. Chapter 1 - Bone Morphology and Organization, Basic and Applied Bone Biology. Academic Press, San Diego, pp. 3-25.

Charan, J. and Kantharia, N.D., 2013. How to calculate sample size in animal studies? Journal of Pharmacology & Pharmacotherapeutics. 4, 303-306.

Chattah, N.L., Sharir, A., Weiner, S. and Shahar, R., 2009. Determining the elastic modulus of mouse cortical bone using electronic speckle pattern interferometry (ESPI) and micro computed tomography: a new approach for characterizing small-bone material properties. Bone. 45, 84-90.

Cho, J.H., Kim, H.C., Suh, C.O., Lee, C.G., Keum, K.C., Cho, N.H., Lee, I.J., Shim, S.J., Suh, Y.K., Seong, J. and Kim, G.E., 2005. Optimum Radiotherapy Schedule for Uterine Cervical Cancer based-on the Detailed Information of Dose Fractionation and Radiotherapy Technique. Radiat Oncol J. 23, 143-156.

Crezee, J., van Leeuwen, C.M., Oei, A.L., van Heerden, L.E., Bel, A., Stalpers, L.J., Ghadjar, P., Franken, N.A. and Kok, H.P., 2016. Biological modelling of the radiation dose escalation effect of regional hyperthermia in cervical cancer. Radiat Oncol. 11, 14.

Damilakis, J., Adams, J.E., Guglielmi, G. and Link, T.M., 2010. Radiation exposure in X-ray-based imaging techniques used in osteoporosis. Eur Radiol. 20, 2707-14.

Douglas, B.G. and Fowler, J.F., 1976. The effect of multiple small doses of x rays on skin reactions in the mouse and a basic interpretation. Radiat Res. 66, 401-26.

Festing, M.F., 1999. Warning: the use of heterogeneous mice may seriously damage your research. Neurobiol Aging. 20, 237-44; discussion 245-6.

Fischer, A.H., Jacobson, K.A., Rose, J. and Zeller, R., 2008. Hematoxylin and eosin staining of tissue and cell sections. CSH Protoc. 2008, pdb.prot4986.

Fowler, J.F., 2010. 21 years of biologically effective dose. Br J Radiol. 83, 554-68.

Glatt, V., Canalis, E., Stadmeyer, L. and Bouxsein, M.L., 2007. Age-related changes in trabecular architecture differ in female and male C57BL/6J mice. J Bone Miner Res. 22, 1197-207.

Green, D.E. and Rubin, C.T., 2014. Consequences of irradiation on bone and marrow phenotypes, and its relation to disruption of hematopoietic precursors. Bone. 63, 87-94.

Hall, E.J. and Giaccia, A.J., 2012. Radiobiology for the Radiologist, Wolters Kluwer Health/Lippincott Williams & Wilkins.

Halloran, B.P., Ferguson, V.L., Simske, S.J., Burghardt, A., Venton, L.L. and Majumdar, S., 2002. Changes in bone structure and mass with advancing age in the male C57BL/6J mouse. J Bone Miner Res. 17, 1044-50.

Halperin, E.C., Brady, L.W., Perez, C.A. and Wazer, D.E., 2013. Perez & Brady's Principles and Practice of Radiation Oncology, Wolters Kluwer Health.

Hamilton, S.A., Pecaut, M.J., Gridley, D.S., Travis, N.D., Bandstra, E.R., Willey, J.S., Nelson, G.A. and Bateman, T.A., 2006. A murine model for bone loss from therapeutic and space-relevant sources of radiation. J Appl Physiol (1985). 101, 789-93.

Hu, M.I., Gagel, R.F. and Jimenez, C., 2007. Bone loss in patients with breast or prostate cancer. Curr Osteoporos Rep. 5, 170-8.

Hui, S.L., Slemenda, C.W. and Johnston, C.C., Jr., 1988. Age and bone mass as predictors of fracture in a prospective study. J Clin Invest. 81, 1804-9.

Jilka, R.L., 2013. The relevance of mouse models for investigating age-related bone loss in humans. J Gerontol A Biol Sci Med Sci. 68, 1209-17.

Khalil, A.A., Bentzen, S.M., Bernier, J., Saunders, M.I., Horiot, J.C., Van Den Bogaert, W., Cummings, B.J. and Dische, S., 2003. Compliance to the prescribed dose and overall treatment time in five randomized clinical trials of altered fractionation in radiotherapy for head-and-neck carcinomas. Int J Radiat Oncol Biol Phys. 55, 568-75.

Maddatu, T.P., Grubb, S.C., Bult, C.J. and Bogue, M.A., 2012. Mouse Phenome Database (MPD). Nucleic Acids Res. 40, D887-94.

Marie, P.J., 1998. Osteoblasts and Bone Formation.

Matsuura, K., Tanimoto, H., Fujita, K., Hashimoto, Y., Murakami, Y., Kenjo, M., Kaneyasu, Y., Wadasaki, K. and Ito, K., 2007. Early clinical outcomes of 3D-conformal radiotherapy using accelerated hyperfractionation without intracavitary brachytherapy for cervical cancer. Gynecol Oncol. 104, 11-4.

Miller, R.A., Austad, S., Burke, D., Chrisp, C., Dysko, R., Galecki, A., Jackson, A. and Monnier, V., 1999. Exotic mice as models for aging research: polemic and prospectus. Neurobiol Aging. 20, 217-31.

Mobbs, C.V., Cheyney, D., Sinha, Y.N. and Finch, C.E., 1985. Age-correlated and ovary-dependent changes in relationships between plasma estradiol and luteinizing hormone, prolactin, and growth hormone in female C57BL/6J mice. Endocrinology. 116, 813-20.

Moore, K.L. and Dalley, A.F., 2006. Clinically Oriented Anatomy, 5th ed. Lippincott WIlliams & Willkins, Philadelphia.

Morris, M., Eifel, P.J., Lu, J., Grigsby, P.W., Levenback, C., Stevens, R.E., Rotman, M., Gershenson, D.M. and Mutch, D.G., 1999. Pelvic radiation with concurrent chemotherapy compared with pelvic and para-aortic radiation for high-risk cervical cancer. N Engl J Med. 340, 1137-43.

Netter, F., 1987. Musculoskeletal system / Anatomy, physiology, and metabolic disorders. 1 8,1 1 8,1, Ciba-Geigy, Summit, NJ.

Nichols, H., 2017. All you need to know about bone marrow. Medical News Today.

NIH Consensus Development Panel on Osteoporosis Prevention, D., 2000. Osteoporosis prevention, diagnosis, and therapy. NIH Consens Statement. 17, 1-45.

Nyman, J.S., Uppuganti, S., Makowski, A.J., Rowland, B.J., Merkel, A.R., Sterling, J.A., Bredbenner, T.L. and Perrien, D.S., 2015. Predicting mouse vertebra strength with micro-computed tomography-derived finite element analysis. BoneKEy Rep. 4.

Oh, Y.L., Yoon, M.S., Suh, D.S., Kim, A., Kim, M.J., Lee, J.Y., Song, Y.J., Ji, Y.I., Kim, K.H. and Chun, S., 2015. Changes in bone density after cancer treatment in patients with cervical and endometrial cancer. J Cancer. 6, 82-9.

Pollack, A. and Ahmed, M.M., 2011. Hypofractionation: Scientific Concepts and Clinical Experiences, LumiText Publishing.

Rotman, M., Sedlis, A., Piedmonte, M.R., Bundy, B., Lentz, S.S., Muderspach, L.I. and Zaino, R.J., 2006. A phase III randomized trial of postoperative pelvic irradiation in Stage IB cervical carcinoma with poor prognostic features: follow-up of a gynecologic oncology group study. Int J Radiat Oncol Biol Phys. 65, 169-76.

Seeman, E., 2002. Pathogenesis of bone fragility in women and men. Lancet. 359, 1841-50.

Shuler, F.D., Conjeski, J., Kendall, D. and Salava, J., 2012. Understanding the burden of osteoporosis and use of the World Health Organization FRAX. Orthopedics. 35, 798-805.

Siegel, R.L., Miller, K.D. and Jemal, A., 2017. Cancer Statistics, 2017. CA Cancer J Clin. 67, 7-30.

Stuben, G., Landuyt, W., van der Schueren, E. and van der Kogel, A.J., 1993. Different immobilization procedures during irradiation influence the estimation of alpha/beta ratios in mouse lip mucosa. Strahlenther Onkol. 169, 678-83.

Teitelbaum, S.L., 2000. Bone resorption by osteoclasts. Science. 289, 1504-8.

Usmani, N., Foroudi, F., Du, J., Zakos, C., Campbell, H., Bryson, P. and Mackillop, W.J., 2005. An evidence-based estimate of the appropriate rate of utilization of radiotherapy for cancer of the cervix. Int J Radiat Oncol Biol Phys. 63, 812-27.

Verhaegen, F., Granton, P. and Tryggestad, E., 2011. Small animal radiotherapy research platforms. Phys Med Biol. 56, R55-83.

Wernle, J.D., Damron, T.A., Allen, M.J. and Mann, K.A., 2010. Local irradiation alters bone morphology and increases bone fragility in a mouse model. Journal of Biomechanics. 43, 2738-2746.

Willey, J.S., Livingston, E.W., Robbins, M.E., Bourland, J.D., Tirado-Lee, L., Smith-Sielicki, H. and Bateman, T.A., 2010. Risedronate prevents early radiation-induced osteoporosis in mice at multiple skeletal locations. Bone. 46, 101-11.

Willey, J.S., Lloyd, S.A., Nelson, G.A. and Bateman, T.A., 2011. Ionizing Radiation and Bone Loss: Space Exploration and Clinical Therapy Applications. Clin Rev Bone Miner Metab. 9, 54-62.

Willey, J.S., Lloyd, S.A., Robbins, M.E., Bourland, J.D., Smith-Sielicki, H., Bowman, L.C., Norrdin, R.W. and Bateman, T.A., 2008. Early increase in osteoclast number in mice after whole-body irradiation with 2 Gy X rays. Radiat Res. 170, 388-92.

Williams, M.V., Denekamp, J. and Fowler, J.F., 1985. A review of alpha/beta ratios for experimental tumors: implications for clinical studies of altered fractionation. Int J Radiat Oncol Biol Phys. 11, 87-96.

Wright, L.E., Buijs, J.T., Kim, H.S., Coats, L.E., Scheidler, A.M., John, S.K., She, Y., Murthy, S., Ma, N., Chin-Sinex, H.J., Bellido, T.M., Bateman, T.A., Mendonca, M.S., Mohammad, K.S. and Guise, T.A., 2015. Single-Limb Irradiation Induces Local and Systemic Bone Loss in a Murine Model. J Bone Miner Res. 30, 1268-79.

Yuan, R., Tsaih, S.W., Petkova, S.B., Marin de Evsikova, C., Xing, S., Marion, M.A., Bogue, M.A., Mills, K.D., Peters, L.L., Bult, C.J., Rosen, C.J., Sundberg, J.P., Harrison, D.E., Churchill, G.A. and Paigen, B., 2009. Aging in inbred strains of mice: study design and interim report on median lifespans and circulating IGF1 levels. Aging Cell. 8, 277-87.